A study of shock-metamorphic features in zircon from the Siljan impact structure, Sweden

Josefin Martell

Dissertations in Geology at Lund University,
Bachelor's thesis, no 482
(15 hp/ECTS credits)

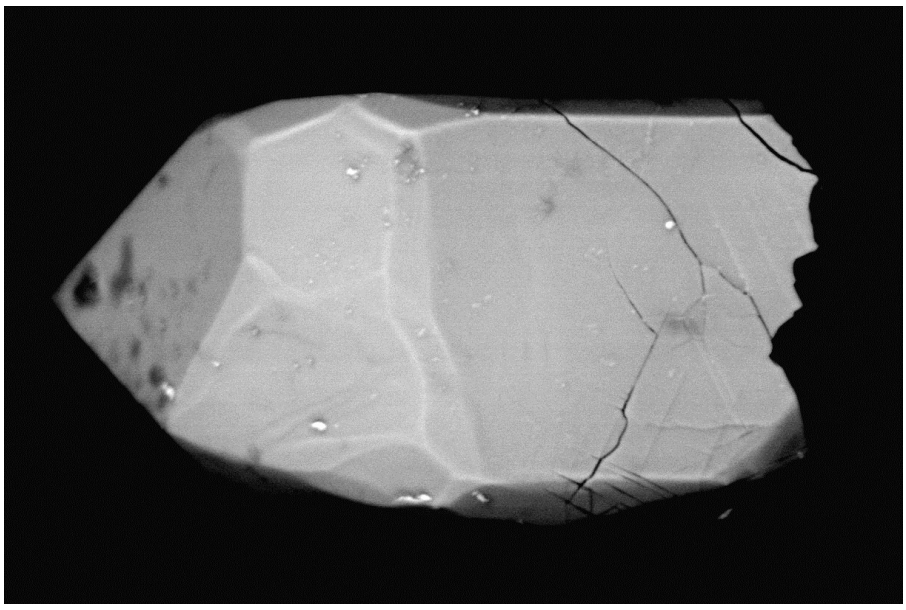

Department of Geology
Lund University
2016

A study of shock-metamorphic features in zircon from the Siljan impact structure, Sweden

Bachelor's thesis

Josefin Martell

Department of Geology
Lund University
2016

Contents

Cover Picture: SEM-image of a zircon grain from sample 54, with visible sets of planar microstructures in lower left corner. Picture by Josefin Martell 2016.

A study of shock-metamorphic features in zircon from the Siljan impact structure, Sweden

Josefin Martell

Martell, J,. 2016: A study of shock-metamorphic features in zircon from the Siljan impact structure, Sweden

Dissertations in Geology at Lund University, No. 482, 23 pp. 15 hp (15 ECTS credits) .

Abstract: Shock-metamorphic features such as planar deformation features (PDFs) and in some cases planar fractures (PFs) are widely used as impact-indicators when to confirm a suspected impact structure. These features only develop when exposed to a sudden and immense pressure and temperature increase in association with meteorite impacts. In previous studies, quartz and k-feldspar containing PDFs have been found at the Siljan impact structure, and the quartz samples enabled an approximation of different shock-zones and the craters original size. In this study, the potential shock-metamorphic effects in the mineral zircon are investigated through scanning electron microscopy (SEM). The samples originate from the Siljan impact structure and are of Järna-granite type. All samples contained planar microstructures, and some of these are assumed to be PDFs based on observations of so-called decorations in the lamellae. The nomenclature on shock-features in zircon is not well established and needs further discussion. However, the findings in this study are in most cases comparable to findings of microstructures in zircon from other impact structures.

Keywords: Zircon, impacts, shock metamorphism, shock metamorphic features, planar deformation features, Siljan impact structure.

Supervisor(s): Carl Alwmark, Sanna Holm-Alwmark, Anderas Petersson

Subject: Bedrock Geology

Josefin Martell, Department of Geology, Lund University, Sölvegatan 12, SE-223 62 Lund, Sweden. E-mail: psy10jm1@student.lu.se

En studie av chockad zircon från nedslagsstrukturen Siljan, Sverige

Josefin Martell

Martell, J., 2016: En studie av chockad zirkon från nedslagsstrukturen Siljan, Sverige. *Examensarbeten i geologi vid Lunds universitet*, Nr. 482, 23 sid. 15 hp.

Sammanfattning:

För att kunna fastställa om en misstänkt nedslagsstruktur verkligen bildats genom ett meteoritnedslag så används så kallade chockstrukturer som *planar deformation features* (PDFs) och i vissa fall *planar fractures* (PFs) som indikatorer. Tidigare studier har visat att kvarts och kalifältspat från nedslagsstrukturen Siljansringen innehåller bland annat PDFs. I denna studie har zirkon från samma lokal undersökts genom svepelektronmikroskopering (SEM). Resultatet visade att samtliga prover innehöll zirkon med *planar microstructures*, och några av dessa kan möjligtvis klassificeras som PDFs. Nomenklaturen för chockstrukturer i zirkon inte lika väletablerad som för kvarts vilket försvårar klassificering av de funna strukturerna. Jämförelser med mikrostrukturer i zirkon från andra nedslagskratrar visar dock att dessa är jämförbara med de från Siljansringen.

Nyckelord: Zirkon, nedslagskrater, chockmetamorfos, impakt, Siljan

Handledare: Carl Alwmark, Sanna Holm-Alwmark, Anderas Petersson

Ämnesinriktning: Berggrundsgeologi

Josefin Martell, Geologiska institutionen, Lunds universitet, Sölvegatan 12, 223 62 Lund, Sverige. E-post: psy10jm1@student.lu.se

1. Introduction

When you look up at the moon at night, you will immediately see that the surface is scarred with impact craters. These constitute an excellent record of the impact rate on the moon through geological time. In contrast, only a handful impact structures are preserved and still observable at the surface of the Earth. For example, no Archean or Hadean-age impact structures have been confirmed even though the cratered surface of the moon shows that the early Earth must have gone through the same bombardment (Cavosie et al. 2010 and references therein). To date, around 190 craters have been identified, and most of them by using shock-metamorphic features in minerals as indicators. These features enable identification even when the impact structure itself is heavily eroded. They can be developed either by the shock-wave produced when a meteorite hits the surface, or during post-impact related events (French 1998).

At the end of the Devonian, approximately 380 Ma years ago (Jourdan & Reimold 2012), a meteorite struck present Dalarna County in Sweden and formed the Siljan impact structure. This is Europe's largest verified impact structure, with an estimated size of 52 km in diameter (Holm et al. 2011). Earlier studies by Holm et al. (2011) have shown that sampled bedrock from the Siljan impact structure contains shock-metamorphosed quartz grains with *planar deformation features* (PDFs) and *planar fractures* (PFs), recording pressures up to 20 GPa. The study also shows that the most strongly shocked quartz grains are located in the center of the structure, and that the distribution of shocked quartz enables an estimation of the original diameter of the crater.

Svahn (2014) continued the study of shock-metamorphic features in minerals from the Siljan area during her bachelor's thesis, and observed shock-metamorphic features in K-feldspar, with the greatest frequency and diversity in samples where pressures have been within the range 15-20 GPa.

1.2 Purpose of this study

The aim of this study is to (1) investigate the occurrence of any shock-metamorphic features in the mineral zircon and (2) compare these features with the previous findings of PDFs and PFs in quartz from the Siljan crater area and other studies on shock-metamorphosed zircon.

This is done by examining zircon grains from three samples from the Siljan impact structure in scanning-electron microscope (SEM), where surface- and interior structures in zircon grains are evaluated. The expectation is, based on earlier studies by (Leroux et al. 1999; Wittmann et al. 2006; Erickson et al. 2012) to find PFs or parallel microstructures.

Few studies of shock-metamorphic features in zircon have been made, and the prospect with this study is to gain better knowledge of zircon-behaviour at high pressures. In the long run this could enable further use of zircon in impact-related contexts, not only in geochronology but also as an impact-indicator along shocked quartz with PDFs.

2. Crater formation

The following paragraphs are based on French (1998) pp 17-22.

In this study, the term *impact-crater* refers to a **hypervelocity impact crater** - a structure formed by a cosmic projectile large enough to remain intact when traveling through the Earth's atmosphere. When striking the ground surface, it has maintained its original cosmic velocity (~>11km/s) and therefore generates intense shock-waves at the point of impact. These pressures can reach several hundred GPa, and are unlike any rock-deforming geological processes normal on Earth (e.g. tectonic and metamorphic processes).

The crater-forming process is generally divided into three steps: **contact and compression, excavation** and **modification** (Fig 1). The first stage begins when the projectile hits the ground surface and transfers an enormous amount of kinetic energy to the target rocks. The shock-waves generated lose energy as they travel away from the point of impact and generally this result in a circular pattern of different "shock-zones". These can be identified by planar microstructures in quartz that can be correlated with shock-pressure. Each shock-zone is characterized by a range of peak pressures and the shock-metamorphic effects apparent in the rocks.

Near the impact rim, velocities drop to about 5-8 km/s and the shock-waves alter to elastic or seismic waves which generates shock-pressures at about 1-2 GPa. At this level the pressure does not produce any permanent deformation in the rocks, but it may generate fracturing, faulting etc. These effects can be hard to distinguish from those produced by normal geological processes.

The contact- and compression stage does not last longer than a few seconds for large projectiles, and less than a second for smaller meteorites. This is the only stage where the projectile itself plays a major role, and when the rarefaction wave (or release wave) has reached the front of the projectile the actual crater excavation is due to the shock-waves expanding in the bedrock.

The two following crater forming stages describe the actual excavation of the crater, where the crater is formed by hemispherical shock-waves expanding from the impact point and through the target rocks. This complex process results in a symmetric excavation flow surrounding the center of the new structure. The material moves differently depending on location, resulting in a bowl-shaped depression in the target rocks. When the crater has reached its maximum size the modification stage begins, and the immediate part where major changes occur lasts approximately a couple of minutes depending on the size of the projectile.

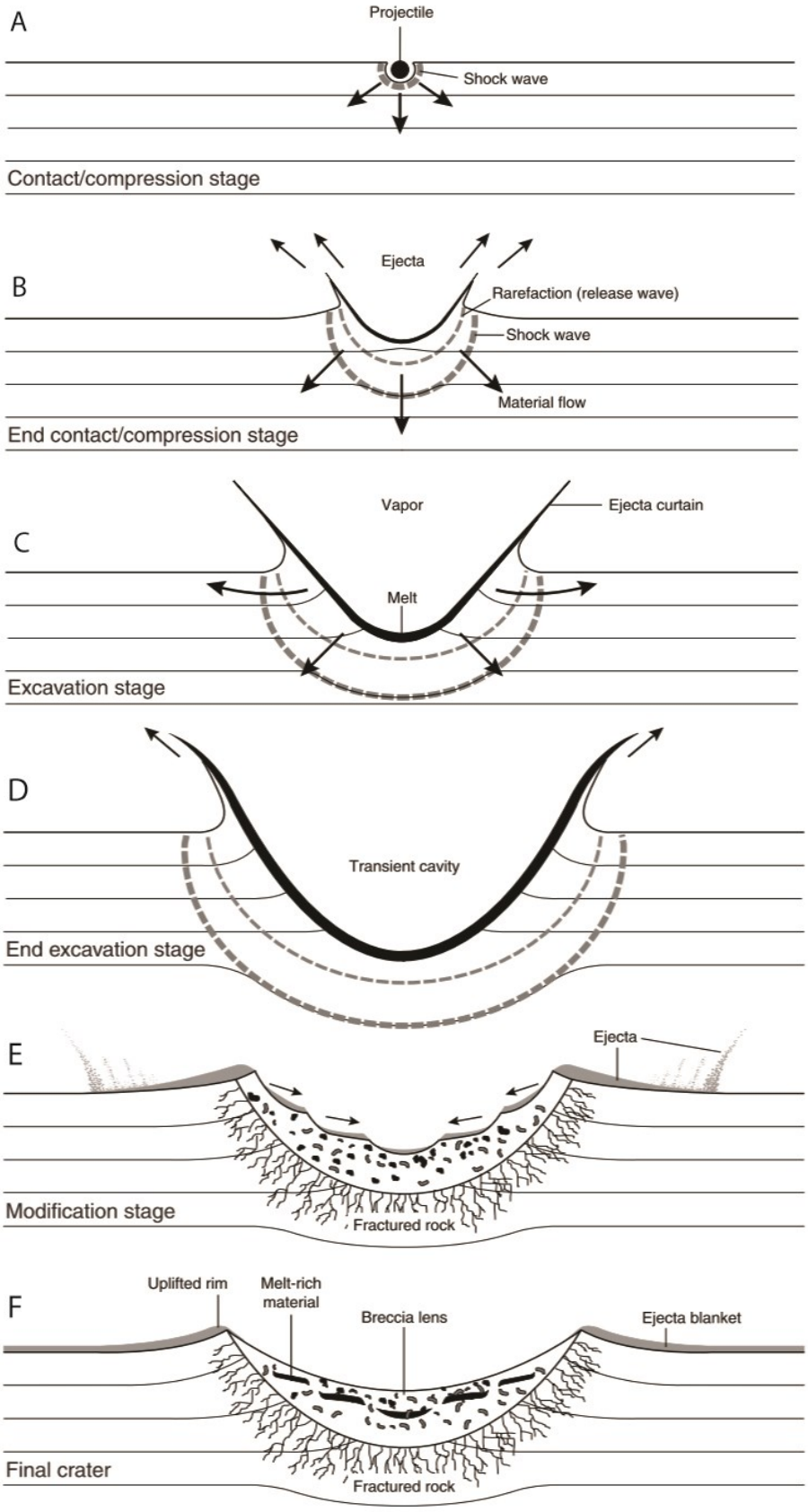

Figure 1 Illustration showing the three major stages during crater formation. Modified from French (1998)

Symptomatic for this stage is rock modification by factors such as gravity and rock mechanics rather than stress produced by shock-waves. Examples include uplift and collapse in and around the rim, erosion and sedimentation. This could go on for a very long time and the modification stage do not have a definite end.

Impacts are near-surface processes; deformation is greatest close to surface and weakens with depth, but shock-effects may extend a few kilometres below ground. The crater is often filled by younger sediments, burying the original structure.

2.1 Identification of impact craters

The identification of shock-effects in minerals is one diagnostic feature when to confirm a suspected impact structure. These specific shock features only form during extreme pressure and heat in association to meteorite impacts. The nomenclature for shock features in quartz is well-established, and two structures that are commonly associated with impact are PFs (*crystallographically controlled planar fractures*) and PDFs *(planar deformation features*) (Erickson et al. 2012). Studies of shocked quartz have been widely used as an indicator within the field of impact cratering, since quartz do not form cleavage under tectonic stress conditions (Timms et al. 2012). During the early 1960s a criteria for establishing the impact origin of suspected impact structures was to identify the transformation to high-pressure polymorphs. Still, the formation of coesite from quartz, and in rare cases redeite from zircon may be used as indicators since none of these minerals are known as a result of e.g. a volcanic eruption or other geological processes where pressure and/or temperature can be high. However, e.g. coesite may form at great depths (with a static pressure of >2 GPa) and later be transported and found at the surface (French 1998).

3. Shock-metamorphism in minerals

In order to understand the process of shock-metamorphism in minerals, it is helpful to first review the basics of shock-wave physics. At the point of impact, a shock wave is built up by an almost discontinuous jump between two stress levels. High pressure is built up at the shock-front and this "boundary" moves at supersonic velocity. The material that is engulfed by the shock-front moves behind it in a lower velocity; this is a so-called high-speed material flow which a characteristic of shock waves. Another characteristic is the residual heating (or waste heat) of the shocked material that derives from the pressure release that takes place after shock compression (Forbes 2012).

A way to illustrate a shock wave and its implications on a material is by the Hugoniot curve (Fig 2). It describes the yield conditions for elastic behavior in different materials with pressure (P) on the y-axis and specific volume (V) on the x-axis, and defines the locus of all shock states that are possible for a given material. It is important to note that the Hugoniot line do not represent the actual path followed by a material during a shock-event and data for each different mineral or material is obtained by experimental studies (Stöffler 1972).

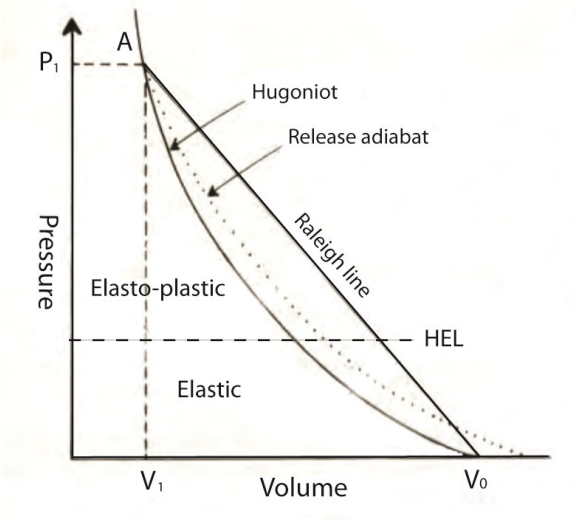

Figure 2 A generalized Hugoniot diagram. Modified from Stöffler (1972)

As seen in Fig 2, the material is compressed along the Raleigh-line (line V0-A) until it reaches the final state A, P1, V1 (peak shock) and is thereafter decompressed along the adiabat line. The area between those lines represents the waste heat from the shock process (Forbes 2012) . The Hugoniot curve can be divided into regions where different deformation processes takes place, most importantly the elastic and the plastic region (Bischoff & Stoeffler 1992). The *Hugoinot elastic limit* (HEL) marks the transition between elastic and plastic behavior of a material exposed to a shock wave.

Based on release adiabat data, it is possible to predict the products of a mineral shocked to various states along the curve. Stöffler & Langenhorst (1994) have correlated shock stages on the Hugoniot curve for quartz with release states at zero pressure, and based on this correlation established two pressure regimes and their typical shock-induced planar microstructures:

Low Pressure Regime (quartz is still crystalline)

- Planar fractures and PDFs (parallel to low index crystallographic planes)
- Decorated and non-decorated PDFs

High Pressure Regime (amorphous phases of quartz, in combination with crystalline polymorphs)

- High-pressure polymorphs (e.g. coesite for quartz)
- Liquid and vapor
- Diaplectic quartz glass (amorphized quartz)

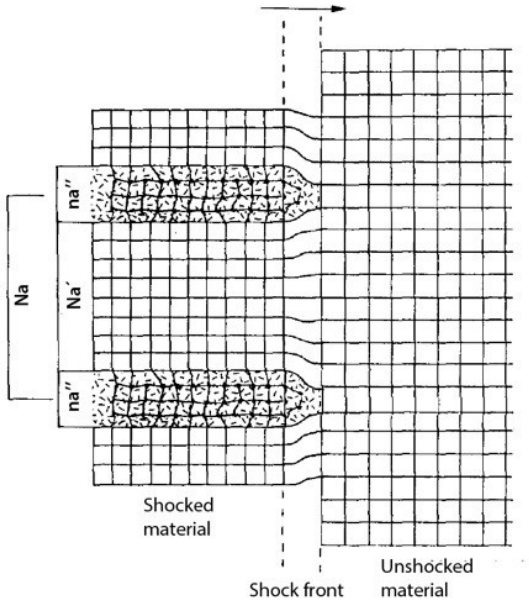

Figure 3 Development of PDFs. Picture shows two regimes with unshocked material in front of the shock-wave and shocked material behind the shock-wave. Amorphous lamellae grow at the shock front (*na''*). Modified from Goltrant et al. (1992)

Experimental studies have shown that PDFs most commonly are parallel to low Millers indicies (MI), and some general orientations are {1013}, {1012}, {1011} and (0001). These orientations give an indication of peak shock-pressure in natural samples, as PDFs parallel to e.g. {1013}occurs at pressures of 10-12 GPa and {1011} within a range of 5-10 GPa (Dressler et al. 1998).

3.1 Formation of PDFs and PFs

PDFs form when a mineral is exposed to a high-temperature and pressure increase that causes melting. The higher shock-intensity of the impact shockwave, the higher temperature and greater chance of localized melting in the mineral. When cooling, the melt will revert to glass (Goltrant et al. 1992). It's more difficult to explain why these melts do occur in straight and specific crystallographic planes, Goltrant et al. (1992) suggests that the reason for PDFs in quartz might be that a particular formation process would favour amorphization in specific $(10\bar{1}n)$-planes, e.g. due to instability of the shear moduli of quartz in some planes. With increasing pressure, the energy of the Si-O-Si bonds decreases in these planes and they are more easily broken, leading to a disorganization of the atoms and thus the formation of amorphous silica lamellae. This formation process is driven by the front of the shockwave and takes place very rapidly. The explanation behind the thin and narrow PDF lamellae can be depicted as in fig 3, where the shock-front moves at supersonic velocity and represents a sharp boundary between a region of unshocked material and a region of shocked material that contains amorphous lamellae.

In some phase boundaries incompatibility between crystal lattices can be relaxed by misfit dislocations that are regularly spaced in the boundary, such as with the exsolution lamellae of clinopyroxene in an orthopyroxene matrix. In the case of PDFs, the phase boundary moves too fast for the incompatibility between the lattices on either side of the shockwave to be fitted in a regular manner. The only way to match these two regions, behind and in front of the shockwave, is the growth of thin and denser amorphous lamellae at the shock front i.e. PDFs. In figure 3, the unshocked material has a unit surface and a height of N lattice planes with a repeated spacing a. This can be compared to the shocked material with N lattice planes, with a spacing $a' < a$ due to elastic compression of the shocked material. If combined with the denser amorphous phase, in the figure represented by na'' where n is the number of compressed lattice planes in the lamellae, the following relation between the two regions on either side of the shock-front can be described as

$$Na = Na' + na''$$

As shown by Goltrant et al. (1992) this formula is used for setting up an expression of the system's energy, and results in the following conditions between the variables of interest:

$$N = \frac{2E}{\propto a}\frac{\Delta a}{a} \text{ and } \frac{n}{N} = \frac{\Delta a}{a''}$$

where E is the variation of the Gibbs energy per unit volume. As E must depend on maximum temperature and pressure, the conclusion is that the density of the PDFs should increase with shock-pressure (Goltrant et al. 1992). These kinds of fresh amorphous lamellae are found in unaltered impact-craters as the Barringer meteor crater and in experimentally shocked samples (French 1998). For a more detailed explanation of PDF formation and concluding equations, please read the publication by Goltrant et al. (1992).

In altered and metamorphosed quartz-samples, the amorphous material in the PDFs has recrystallized back to quartz, and the lamella instead contains fluid inclusions visible as tiny bubbles or "decorations". The crystallographic orientations are however preserved and the resulting feature is so called *decorated* PDFs (French 1998). These bubbles probably forms during water-precipitation at a post-shock thermal event (Goltrant et al. 1991).

In the nomenclature for impact-structures in quartz, PFs are described as sets of open parallel fractures, cleavage or cracks that develop at the lowest shock-wave pressure ranges (~5-8 GPa). They are usually more widely spaced than PDFs in quartz grains, and cleavage similar to these fractures can occur in quartz from non-impact settings. Because of this, PFs in quartz are not used independently as an impact criteri-

on but can be used as an impact-indicator along other impact related features (French 1998). Engelhardt & Bertsch (1969) describe planar fractures as open fissures, or fissures filled with secondary minerals, arranged in a wider and more irregular pattern than PDFs. Both PDFs and PFs tend to concentrate along corners and grain boundaries, and do not have to penetrate the entire grain (Engelhardt & Bertsch 1969)

4. Zircon ($ZrSiO_4$)

Zircon ($ZrSiO_4$) belongs to the tetragonal crystal system and is an accessory mineral in sedimentary, igneous and metamorphic rocks, though most common in igneous rocks with a quartz saturated composition (Hoskin & Schaltegger 2003). It is known to contain trace elements such as uranium and thorium since these can substitute for Zr^{4+} and Si^{4+}, and the presence of radioactive mother isotopes enables geochronological dating according to the U-Pb method (Harley et al. 2007; Davis et al. 2011).

The durability of zircon crystals and their ability to withstand erosion, and further their capability to incorporate trace elements is mainly due to the crystal structure, where various minerals that are isostructural with zircon can take T- and A-site cations within its general formula ATO_4. These include for example silicates, vanadates and phosphates, all belonging to the zircon-group of minerals (Finch & Hanchar 2003).

4.1 Previous studies of microstructures in zircon

It is relatively easy to determine the orientations of planar deformation features in quartz because of its uniaxial optical character. Other benefits include its transparency and lack of cleavage (Bohor et al. 1993). However, in old and eroded impact craters as the Vredefort Structure, crucial features in quartz may be absent due to post-impact thermal and hydrothermal processes (Leroux et al. 1999).

According to Leroux et al. (1999), shock-effects in zircon such as granular (or "strawberry") textures and planar features are classified as shock features. Granular textures in zircon result from shock-induced amorphization, and is represented by zircon crystallites in a $ZrSiO_4$ matrix (Wittmann et al. 2006). Other shock-induced deformation features include planar microstructures such as dislocation patterns and interpenetrating micro-cleavage (in this paper referred to as PFs) (Leroux et al. 1999). However, Leroux et al. (1999) state that the true nature of these planar features is poorly understood.

In an experimental study by Leroux et al. (1999) zircon was shock-deformed at 20, 40 and 60 GPa in order to establish in which pressure range these different deformation effects are produced. At 20 GPa, they observed micro-cleavage, and observations of dislocations in glide configuration indicated plastic deformation. These micro-cleavages are developed during the compression stage and form due to shear stresses and occurred mainly in (100) planes.

At 40 GPa, parts of the sample was transformed into a scheelite-type structure (denser crystal structure, in zircon referred to as reidite) and were observed in some grains that had not yet been transformed.

At 60 GPa, the entire sample was transformed to the scheelite-structure phase, and cross-cutting showed that PDFs were formed in the zircon-structure before the phase change took place.

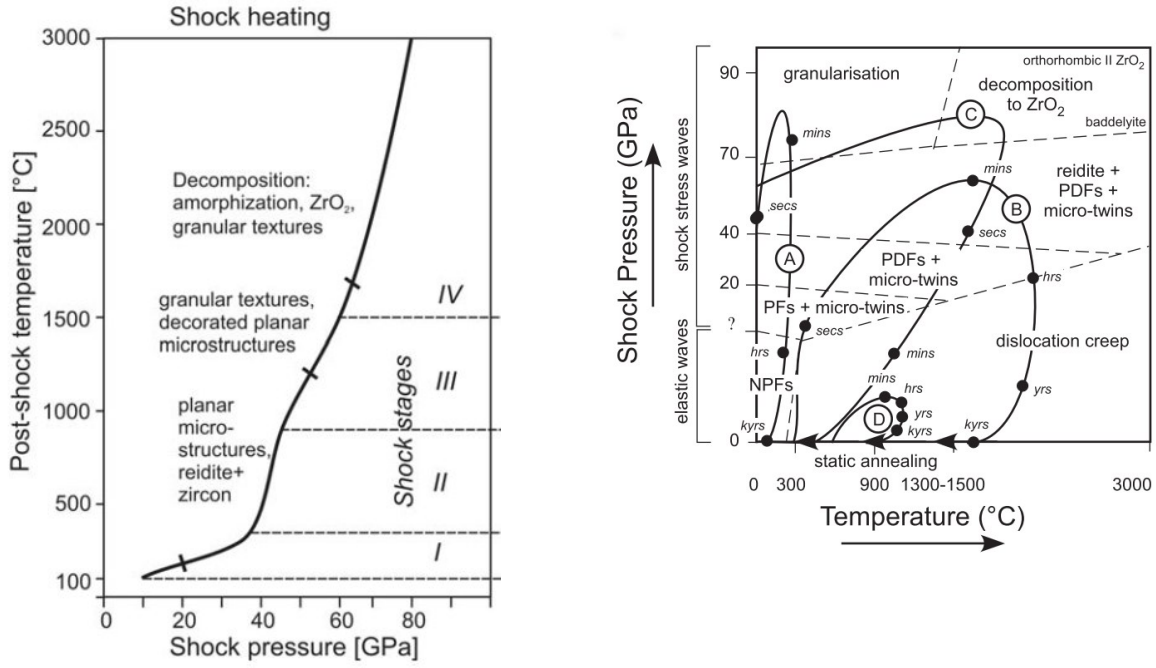

Figure 4 (left) Stability ranges of shock features in zircon (modified from Wittmann et al 2006) and (right) Shock-deformation mechanism map (modified from Timms et al 2012)

Based on the experimental shock-studies of zircon behaviour (Leroux et al. 1999), in combination with data on relative proportions of shock microstructures in zircon from different sites within crater formations, Wittmann et al. (2006) compiled a diagram showing stability ranges of shock features in zircon with post-shock temperature on the y-axis as a function of shock pressure (fig 4). Noteworthy is that the transition from zircon to reidite and the formation of planar microstructures starts at approximately 20 GPa. The transition to reidite is complete at 52 GPa, where instead amorphization (structural breakdown) and granular aggregates are observed.

As mentioned in the publication by Timms et al. (2012), the pressure-temperature diagram by Wittmann et al. (2006) implies an approximate linear relation between post-shock temperature and shock-pressure. Timms et al. (2012) thus continued the diagram with the pressure and temperature plotted over time, resulting in an approximate schematic "shock-deformation mechanism map" (Timms et al. 2012) for zircon (Fig 4). The loops drawn on the diagram represents hypothetical turns by a zircon grain in different locations, based on temperature and pressure in specific timeframes during an impact event. If PFs are to be impact-related, this requires tensile or shear stress and high strain rates during a very short timeframe, possibly less than a few seconds. The diagram also suggests that one zircon grain can develop several different microstructures related to one single impact-event, which could be important when describing grains with overprinting sequences of microstructures and further enables identification of several events during one single impact.

Erickson et al. (2012) found that zircon grains from the Vredefort dome structure contained PFs in seven orientations; {010}, {100} and {011} and four orientations of {112}. These were identified by correlating external and internal microstructures of the grains. In zircon-samples from the same location they also identified so called micro-twins. These generally occur

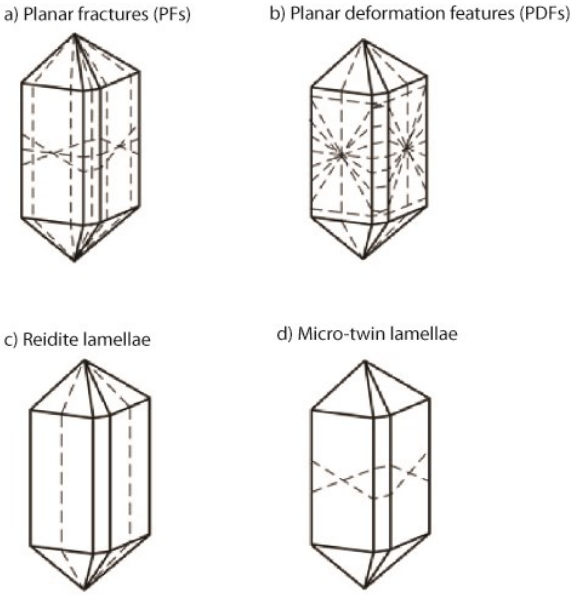

Figure 5 Image showing various crystallographic orientations in zircons with a) PFs b) PDFs c) reidite lamellae and d) micro-twin lamellae. Modified from Timms et al. (2012)

oriented with a 65º rotation about <110> and consist of several parallel sets of thin lamellae (Fig 5 and Fig 6). Timms et al. (2012) found micro-twins in lunar zircon that was formed simultaneously with PFs in (112), as a shear response to compression or extension.

Zircon survive as a shocked mineral at pressure ranges up to ~20 GPa where it transforms to its high-pressure polymorph reidite; a diagnostic of impact. Its tetragonal structure is similar to that of zircon, but its density is increased ~10% compared to zircon.

The polymorph reidite was first reported from high-pressure experiments by Reid & Ringwood (1969), and pressure-ranges where it remains stable has since then been established. Reidite reverts to zircon above ambient pressure at 1200°C (Kusaba et al. 1985).

Naturally formed reidite has only been reported

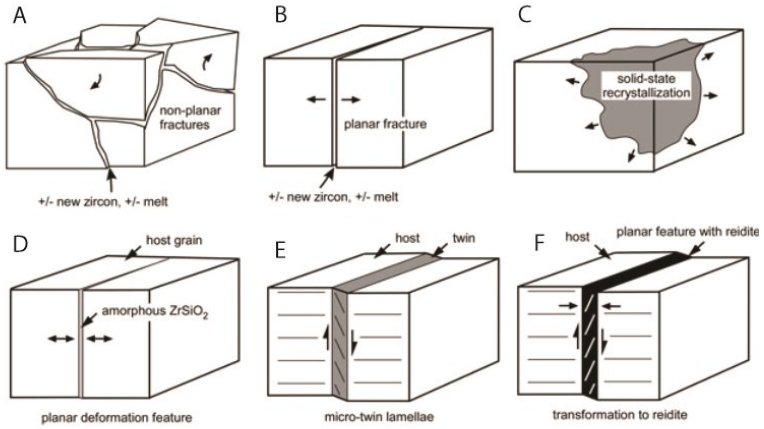

Figure 6 Schematic illustration showing the formation process of different microstructures. Modified fromTimms et al. (2012)

from a handful sites globally, where all have been relatively young impact craters (<36 Ma) (Cavosie et al. 2015). It was found among e.g. tektite glass, shocked quarts, coesite and stishovite at the Eocene Chesapeake Bay impact site (Wittmann et al. 2006). Cavosie et al. (2015) suggests that if identified, natural occurrence of reidite in ancient Hadean zircons may provide evidence of early impact-events on Earth.

5. Geological setting

The Siljan impact structure is approximately 52 km wide and located in Dalarnas län in South-central Sweden. The bedrock in the area is made up by crystalline rocks, mainly Dala-granite of Järna and Siljan types (Fig 7), superimposed with Ordovician and Silurian sediments. For a more detailed description of the regional geology the reader is referred to the publication by Holm et al. (2011).

Heavy erosion has changed the morphology of the formation, which has led to exposure of levels that lied below the original floor of the crater. Silurian and Ordovician sediments are preserved in the circular depression, now filled with lakes (Siljan and Orsa lake), that together forms the so-called Siljan Ring. The area within the circular depression consists of crystalline rocks, and is the only remnant from the central plateau that formed after the collision (Holm et al. 2011).

6. Materials and methods

This study is based on three rock samples, collected from different locations in the Siljan area (fig 7). The rock samples were crushed into fine-grained powder using a sledge hammer and a swing mill. Water was added and the sample loaded to a Wilfley-Holman 700 water-shaking table in order to separate heavy minerals, following the method by Söderlund & Johansson (2002). From the resulting sample, magnetic minerals were removed with a magnetic pencil and zircons were handpicked from a petri dish using a pipette under a binocular microscope. The quality and size of the zircon grains varied within the samples, and the most euhedral ones were picked for imaging. About thirty to fifty grains were picked from each sample and mounted on coal tape.

To describe shock-metamorphic surface features of the zircon grains, backscatter electron (BSE) - and secondary electron (SE) imaging was carried out with a Hitachi 3400N scanning-electron microscope (SEM) at the department of Geology, Lund University, Sweden. A second SEM-analysis was made after all grains were cast in epoxy and polished to mid-plane to expose a cross-section within each grain. The purpose of the second analysis was to establish internal features, such as PFs. All three samples were evaluated and characterized from their significant shock-features and are presented in this report.

Figure 7 Map showing the Siljan impact structure. Pink area indicates bedrock of Järna-granite type. Blue dots indicate locations for sample 54 and the Hättberg-samples (Modified from Holm et al 2011)

6.1 Previous studies

Holm et al. (2011) have previously examined PDFs in quartz from the Siljan area. Shocked quartz grains were used to determine the shock-center of the Siljan impact structure based on PDF findings in quartz grains from different shock-zones.

Based on the distribution of shocked quartz the original diameter of the eroded crater could be estimated to 90 km.

6.2 Samples

All samples were collected by Sanna Holm-Alwmark & Carl Alwmark and described in Holm et al. (2011). **Sample 54** is collected from the surface and the *Hättberg-samples* are obtained from a drill–core at **5 m** and **451 m** respectively; these are referred to as sample 5 and sample 451 (Table 1).

Table 1 Sample descriptions

Sample no	Zircon grain size (µm)	Colour of zircon grains	Comments on rock sample
54	45 to 140 µm	Yellow- to transparent	Rock-sample is of Järna-granite type, red in colour. Medium to coarse-grained.
Hättberg			
5	30 to 75 µm, with a few exceptions where grain size was approximately 100 µm	Transparent	Rock-sample is of Järna-granite type and attained from a drill core, 5 metres below surface, light red to grey. Medium to coarse-grained.
451	50 to 140, with a few grains reaching up to a size of approximately 170 µm	Transparent- to yellow	Rock-sample is of Järna-granite type and attained from a drill core, 451 metres below surface, red in colour. Medium to coarse -grained.

7. Results

This section includes shorter descriptions from each sample of some of the grains that contain planar microstructures. SEM-analysis showed that all samples contained grains with planar microstructures (Table 2). Statistics on potential microstructures is also included in Table 2. These are zircons that contain microstructures, but where an impact-related origin could not be established. Sample 54 had the highest rate of PMs in total, where approx. 27% of the grains showed one or more sets of PMs. However this sample included more grains than the other two - 55 respective to 32 and 33 for sample 5 and 451. The result from the second SEM-analysis is that most polished midsections did not show any planar microstructures, but a few grains contained vague interior planar features. Orientations of planar microstructures have not been determined; however in cases where the c-axis is distinguishable it is possible to assume plane-orientations in (100), (010) and (001).

SEM-images of all individual grains not included in this section and images of the polished grains from the second SEM-analysis can be found in Appendix A.

7.1 Sample descriptions

Figure 8 and 9 shows examples of grains were the angles of observed PM-sets were measured. Grain 54_1 (Figure 8) and grains A, B and E (Figure 9) intersects the c-axis at approximately 65º . Grains C and D intersects the c-axis at approximately 34º .

7.1.1 Sample 54

Several zircon grains from sample 54 contained planar microstructures; images of seven zircons with planar microstructures (PMs) from sample 54 are described in this section.

Zircon 54_1 is about 50 µm and has at least 4 sets of intersecting planar microstructures. These are all located in one corner of the crystal. One larger fracture is cutting through some microstructures (Figure 8).

Zircon 54_6 has a size of approximately 30 µm and appears to be a part of a larger grain. Two intersecting sets of planar microstructures are visible in the right corner of the grain, even though the surface is rough and full of small marks (Figure 10).

Zircon 54_10 is approximately 50 µm and appears to be a part of a larger grain. Two sets of distinct planar lamellae with possible decorations or "bubbles" are observable at its surface. Some planar lamellae seem to be deformed or "creased" (Figure 11).

Zircon 54_31 is 70 µm and have two observable sets of non-intersecting planar microstructures, one of the

Table 2 Showing results including for example number of grains with confirmed planar microstructures.

First SEM-analysis

Sample no.	Number of grains	Approx. min.-max. size (µm)	Confirmed planar microstructures (%)	Potential microstructures (%)	Number of visible sets (%)*	
					One set	Two sets or more
54	55	45-140	27	29	47	53
5	32	30-100	22	6	57	43
451	33	50-140	18	27	67	33

**in grains with confirmed planar microstructures*

sets run perpendicular to the c-axis (001) (Figure 11).
Zircon 54_48 is a relatively euhedral grain with visible crystal faces, and a size of about 60 µm. It has two observable sets of planar microstructures, one of which cuts through fractures that are running perpendicular to the lamellae (Figure 11).
Zircon 54_14 the observable part of this grain includes both interior and a small fraction of the surface. One set of planar microstructures is visible both at the surface and within the grain (Figure 11).
Zircon 54_11 and ***zircon 54_30*** are two examples of grains that contain some form of parallel lineation, but this lineation differs from the other planar microstructures observed; they are generally shorter and sometimes slightly curved. No surface is visible on grain 54_11, but lineation (presumably along the c-axis of the grain) might indicate planar microstructures. Grain 54_30 contains one set of parallel structures in the lower left corner of the image, running perpendicular to the c-axis (Figure 12).
Zircon 54_40 has one set of very distinct planar microstructures, approximately 30º to the c-axis. The grain is about 60 µm, with a smooth surface and visible crystal faces. At least two fractures run through the grain, and cuts through the lamellae (Figure 12).

7.1.2 Sample 5

22% of the zircon grains from sample 5 contained planar microstructures, which is a lower quantity than for sample 54. Images of two zircons with planar microstructures and one with potential planar microstructures from sample 5 are described in this section.
Zircon 5_13 is a sub-rounded grain with a size of 55 µm (measured along c-axis) and some visible crystal faces. It contains one set of planar microstructures that run close to perpendicular to the c-axis. The structures are observable as vague parallel lines. The surface contains marks and/or voids from several inclusions (Figure 13).
Zircon 5_30 is a rounded grain with visible crystal faces. It is about 50 µm with several fractures that are aligned in the same orientation. One set of planar microstructures is observable perpendicular to these fractures. (Figure 13)
Zircon 5_15 is approximately 50 µm measured along the c-axis. No clear surface is observable. Parallel lineation is visible within the grain, aligned with its c-axis (Figure 14).

7.1.3 Sample 451

18% of the grains from the drill-core sample obtained at 451 meters contain planar microstructures. Images of three zircons with planar microstructures and one with potential planar microstructures from sample 451 are described in this section.
Zircon 451_7 is a 50 µm, fragmented grain with one visible set of planar microstructures (Figure 15).
Zircon 451_18 is an elongated grain, approximately 70 µm along its c-axis. It contains two sets of planar microstructures, both about 40º to the c-axis. One elongated inclusion, dark in color, cuts the grain perpendicular to the c-axis (Fig 10).
Zircon 451_28 is 50 µm with distinct crystal faces. A pyramid-shaped "top" indicates that it is a part of a larger grain. The grain contains planar microstructures perpendicular to its c-axis. These structures are dark in colour and have a homogenous spacing. The lamellae appear as straight lines, however many of the separate lines are "shaky" as a result of former inclusions or decorations. (Figure 15)
Zircon 451_23 appears to be a fragment of a larger grain, where the part visible in the image shows the interior of the grain. It contains parallel marks in different orientations; some of them appear to be parallel, but none are continuous through the grain (Figure 15).

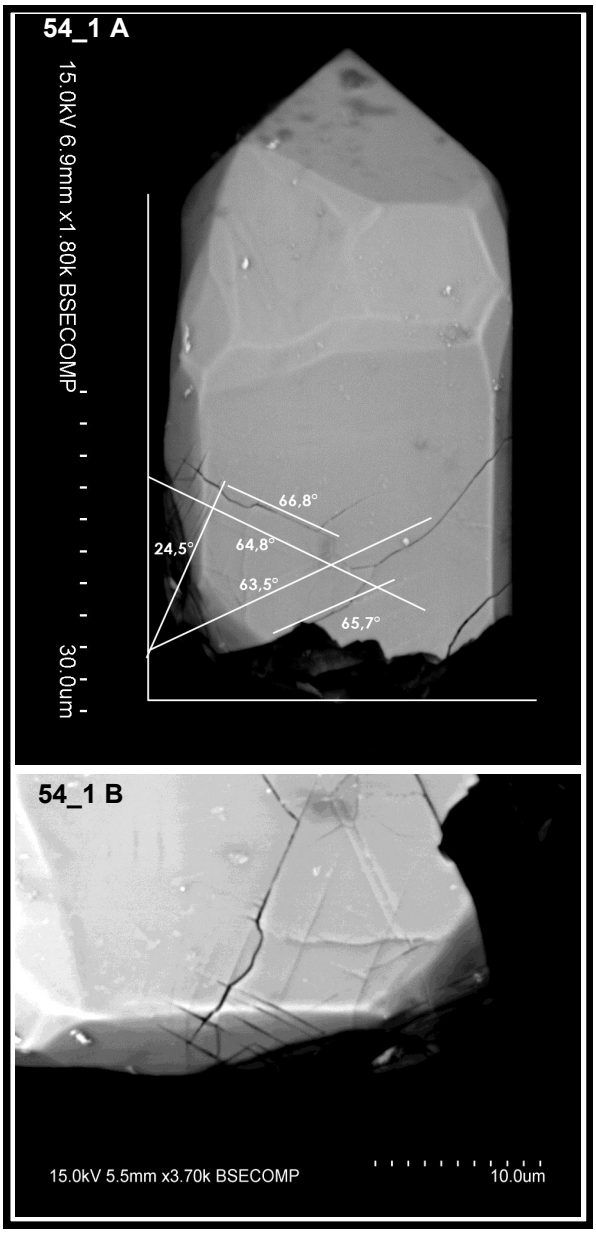

Fig 8 A) Zircon grain with added lines visualizing angles for all sets. The average value is 65º. B) Close-up on the PMs. (SEM-imaging)

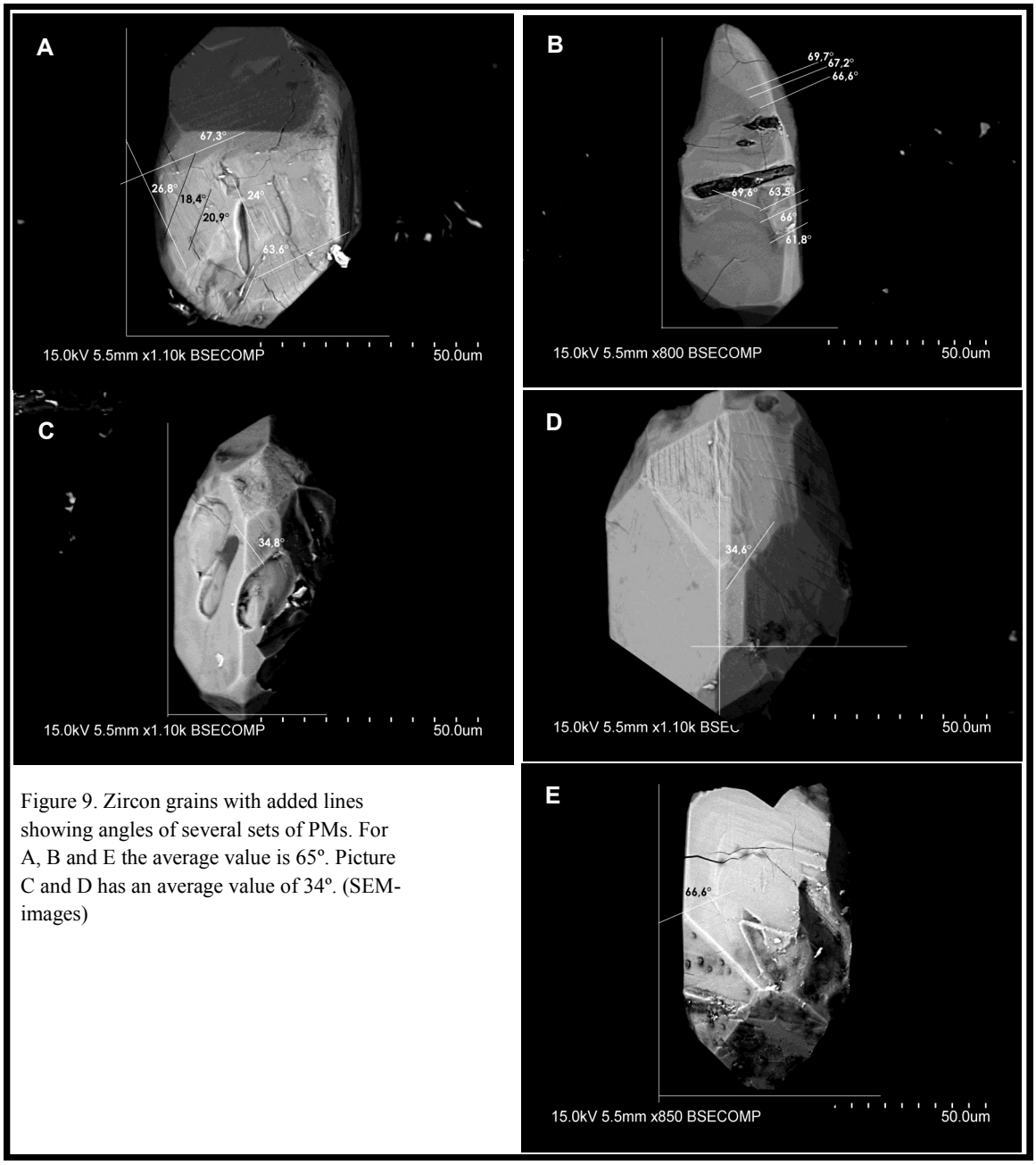

Figure 9. Zircon grains with added lines showing angles of several sets of PMs. For A, B and E the average value is 65º. Picture C and D has an average value of 34º. (SEM-images)

Sample 54

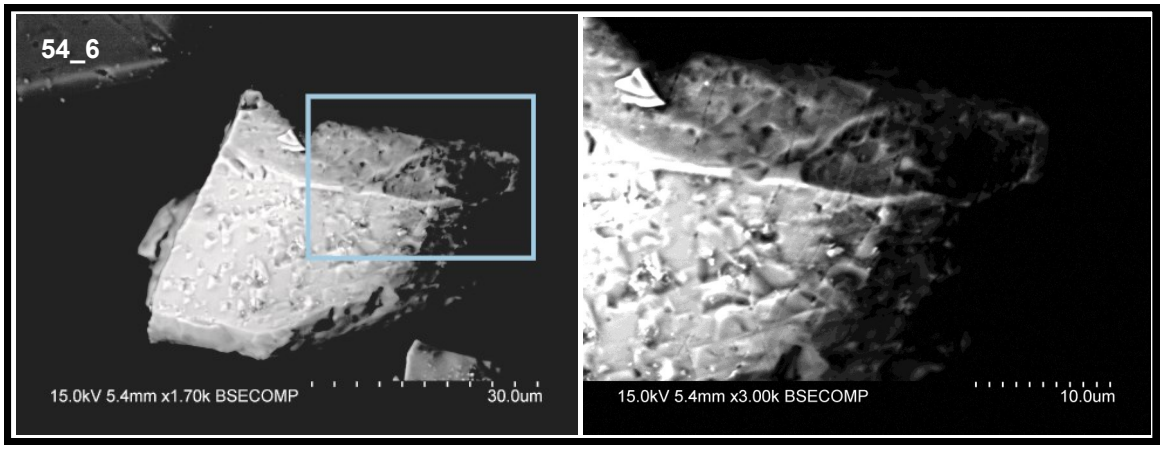

Figure 10 Zircon grain 54_6, second image shows magnification of PMs. (SEM-images)

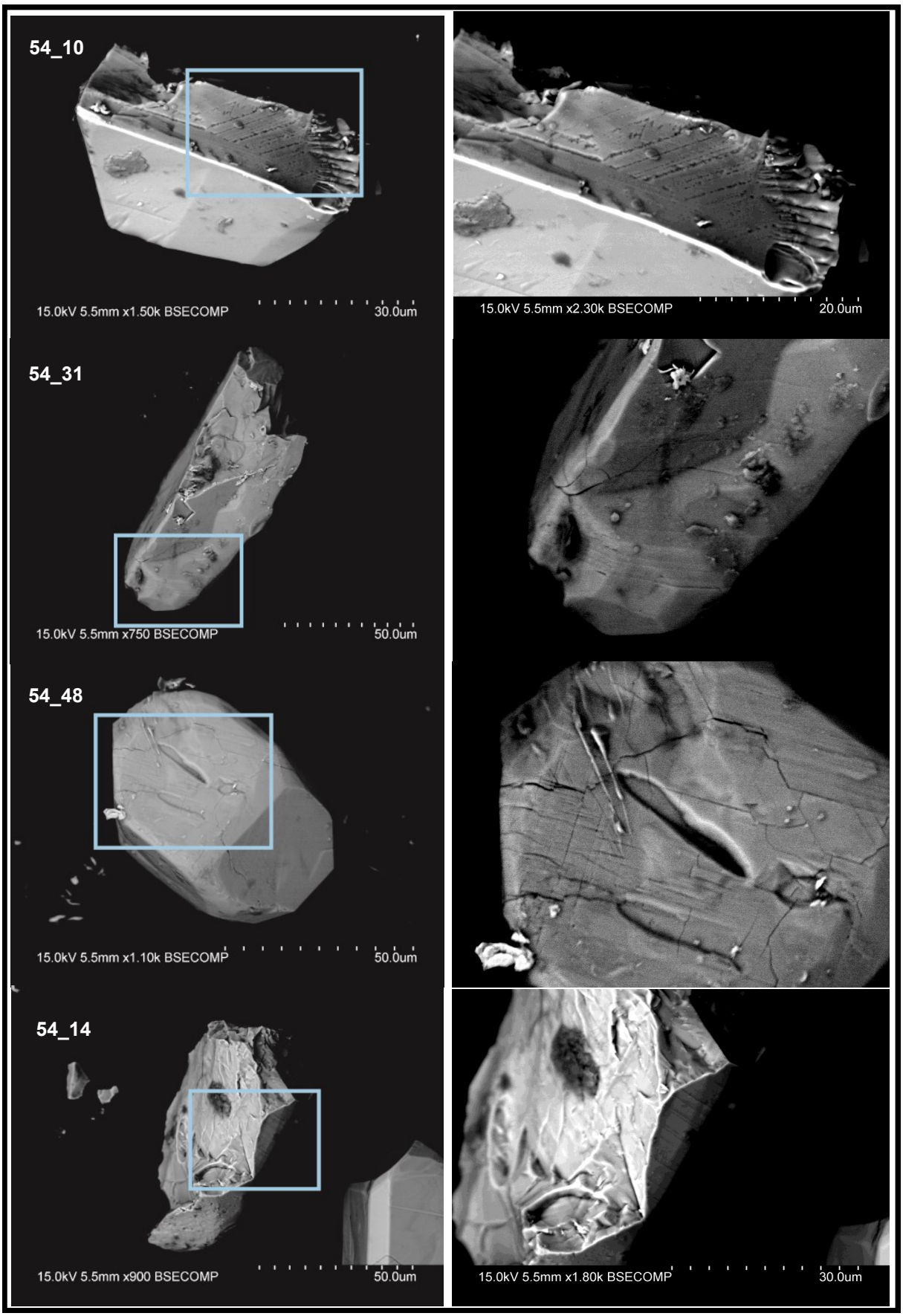

Figure 11 Showing grains 10, 31, 48 and 14. Right column shows magnification of PM-sets. (SEM-images)

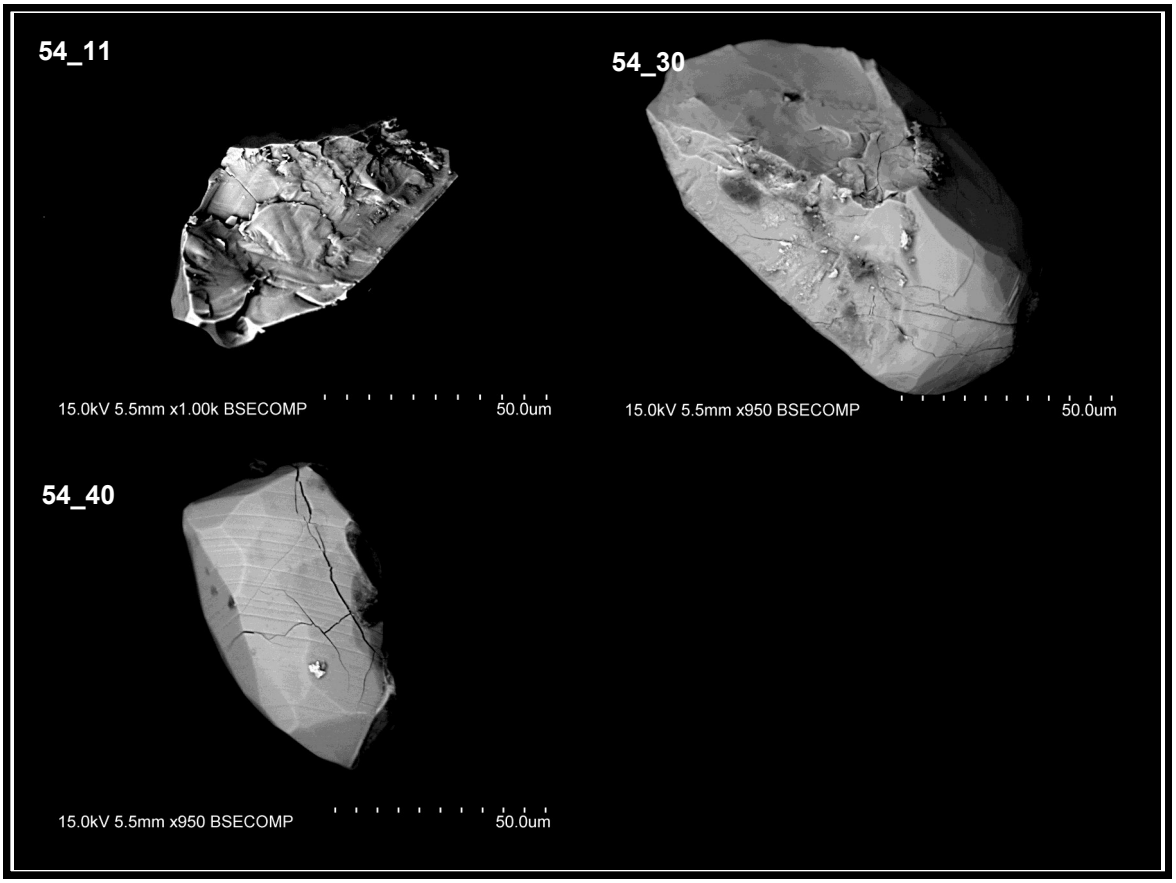

Figure 12 Zircon grains 11 and 30 show potential PMs. Grain 40 contains one distinct set of PMs. (SEM-imaging)

Sample 5

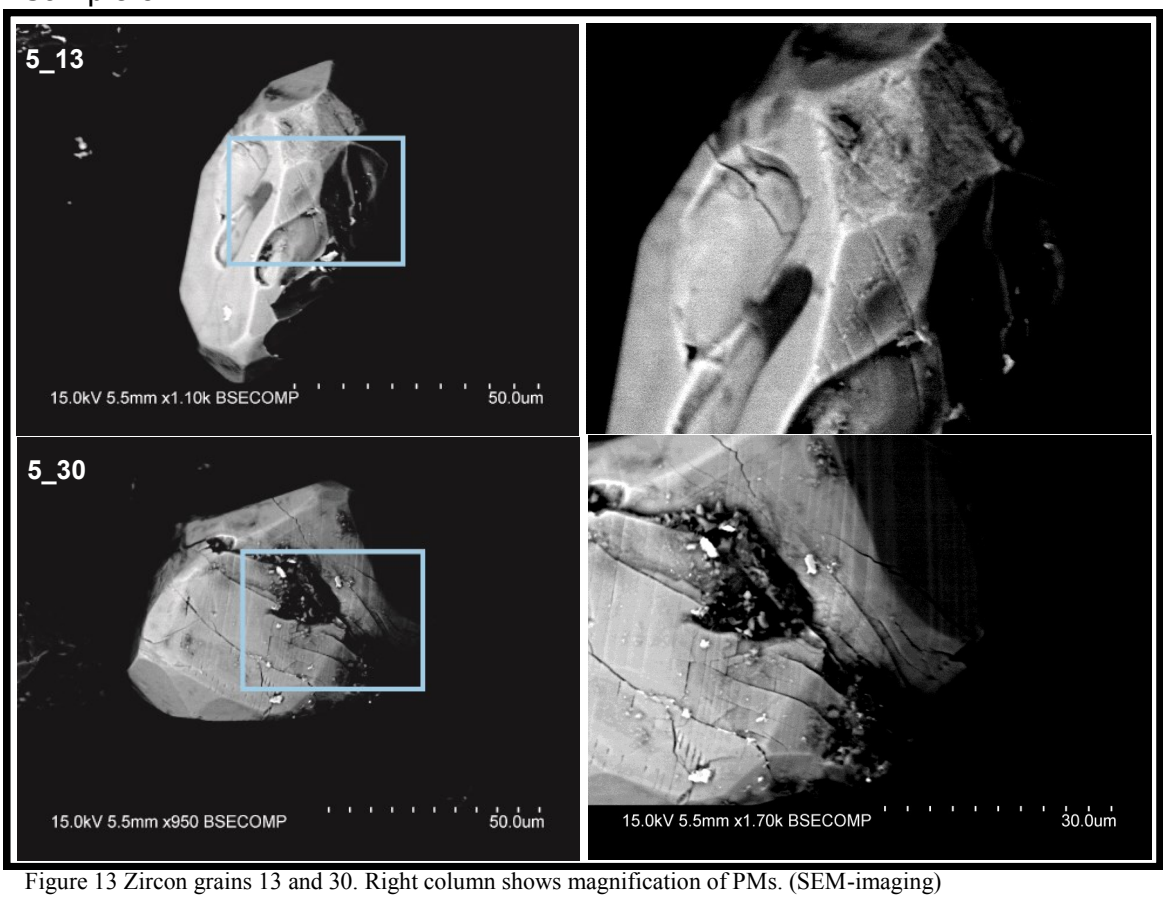

Figure 13 Zircon grains 13 and 30. Right column shows magnification of PMs. (SEM-imaging)

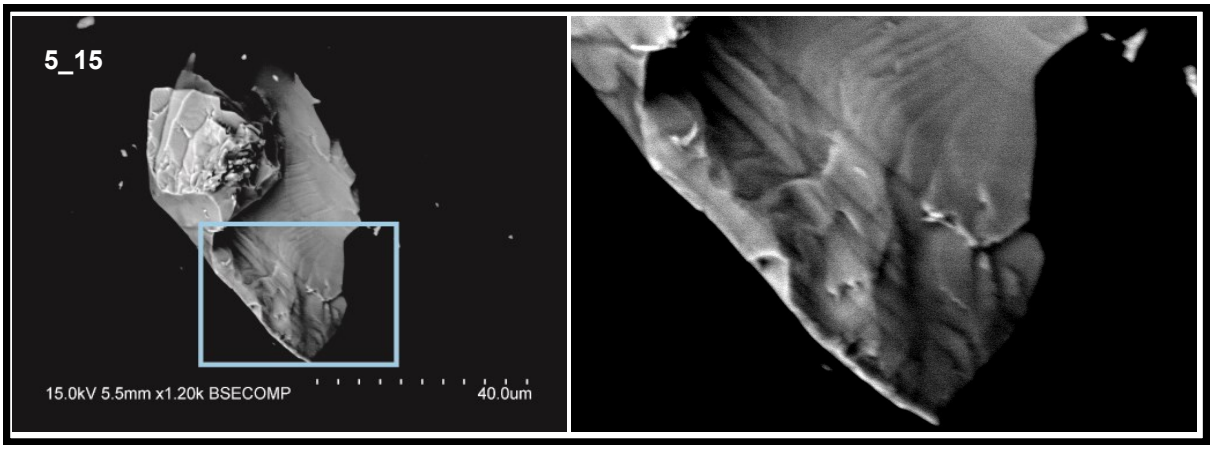

Figure 14 Grain 15, right column show magnification of linear structures.

Sample 451

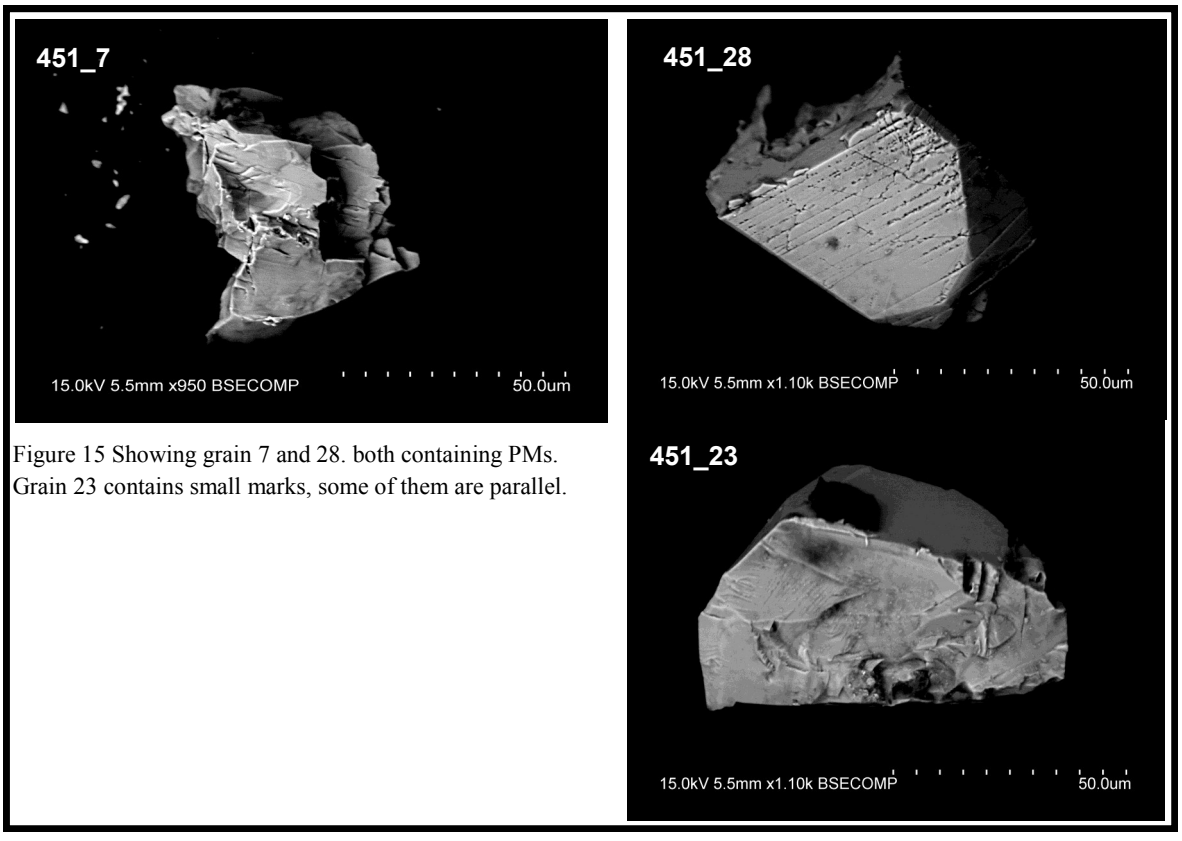

Figure 15 Showing grain 7 and 28. both containing PMs. Grain 23 contains small marks, some of them are parallel.

8. Interpretation and discussion

8.1 Sample discussion

Sample 54 had the highest rate of euhedral grains, with fewer dusty grains. This is also a potential factor that could account for the difference in quantity of shocked grains between the samples, since grains with a heavily eroded surface gave little to no information about surface-structures: it could not be ruled out these grains initially had planar structures at the surface.

SEM imaging showed that the interiors of the grains were fairly smooth and that several grains contained fractures. These fractures were in most cases not parallel and where parallel lineation was observed these were visible as vague bright lines and appeared only in a minor part of the grain.

For the majority of the zircons, orientations of the planar microstructures were not identified. In some cases the c-axis was distinguishable and orientation could be determined to (100), (010) or (001), but further analysis is required. This could be done either by using EBSD or by using an u-stage. Erickson et al. (2012) found that PFs in (100) and (010) were among the first microstructures to develop in shock-metamorphosed zircon. They also found that c-axis parallel planar fractures sometimes were absent in polished sections, suggesting that they may anneal rapidly.

As shown in the map (fig 16) both the Hättberg-samples and sample 54 lies within the estimated shock-range of 10-15 GPa (Holm et al. 2011). Since the shock-pressure decreases with depth, this is not accurate for sample 451. However, it gives an indication of what kind of shock-metamorphic structures you could expect to find in the zircons from the different sample locations. Zircons with lamellae interpreted as decorated PDFs was observed in both sample 54 and sample 451; this would indicate a relatively high shock-pressure (Wittmann et al. 2006). See further discussion on this matter in section 8.2.

The nature of the found lamellae differs, in zircon 54_1 and 54_40 they are vague, and resembles PDFs that only are observable at the surface, grain 54_48, 54_6 and 54_10 seems to have deeply "etched" lamellae that resembles fractures. Figure 12 shows examples of two grains with parallel features, however it's unclear if they are impact-related or not: grain 54_11 does not have a visible grain surface, but some lineation is visible within the grain. Zircon 54_30 has parallel features in the lower right corner, these appear as lighter streaks and are possibly impact-related.

8.2 Origin of microstructures found in Siljan

Using the term PDFs when describing planar microstructures in zircon is controversial. Earlier publications have referred to parallel structures in zircon as either PDFs or in some cases simply as PFs or parallel microstructures. Erickson et al. (2012) suggest that the term PDF should only be used when describing quartz- or zircon ($ZrSiO_4$) grains with amorphous lamellae, and claims this have not yet been identified in any naturally shocked zircon. Amorphous lamellae in zircon was reported by Leroux et al. (1999) in grains that were experimentally shocked at pressures of 40 to 60 GPa. Findings of PDFs in lunar zircon was reported by Timms et al. (2012), based mainly on weakened EBSD bands in their zircon samples, interpreted as an amorphous phase. Erickson et al. (2012) criticized this deduction, claiming that their evidence does not eliminate other explanations for the weakened EBSD bands, and suggest that it also could be a consequence of elevated concentrations of lattice defects. They further propose that all planar microstructures at the surface of or in the interior of the zircon grains should be referred to as PFs if they do not fulfil the traditional criteria's for PDFs in quartz. In their publication they do not mention decorated lamellae as an equivalent to amorphous lamellae when defining and determining PDFs. Wittmann et al. (2006) do however report findings of PDFs in zircon from the Chicxulub crater, and describe these as decorated. Decorations in shocked minerals occur due to post-shock annealing of the amorphous phase, and preserves the original orientation of the amorphous lamellae (French 1998). When to use the term PDF or not seems to be a matter of definition, and based on publications by e.g. Holm et al. (2011) and Wittmann et al. (2006) decorated lamellae will be referred to as PDFs in this report.

In most previous studies, PFs in zircon have been visible both at the surface of and in the interior of the grains (Cavosie et al. 2010). In this report, the observed parallel microstructures in the zircon grains were initially assumed to be PFs and not PDFs, and a

Figure 16 Map over the Siljan crater area. Pink area indicates bedrock of Järna-granite type, blue dots show locations for sample 54 and the Hättberg-samples. Black lines show the different estimated pressure-ranges (Modified and based on Holm et al 2011)

second analysis of each shocked grain was made to support this fact. However, very few of the polished mid-sections of the grains did show any parallel fracturing.

The unexpected result by the second analysis provides three potential scenarios regarding the origin of the observed parallel microstructures at the surface of the grains:

Scenario 1, the described microstructures are PDFs
The pressure range at Siljan location 54 is estimated to 10-15 GPa (Holm et al. 2011), and according to experimental studies by Leroux et al. (1999) and the P-T diagrams by Wittmann et al. (2006); Timms et al. (2012) PDFs in zircon form when shock-pressure is approximately 30-40 GPa. It should be noted that experimental studies are not always analogous to natural events (Stöffler 1972; Langenhorst 2002; Sharp & Decarli 2006). In nature both pressure and temperature tend to be heterogeneous, and according to Stöffler (1972) strain rates and peak pressure duration tend to lower the minimum peak pressure for the development of shock effects in natural impact processes. No approximations of shock-pressures at Hättberg location have yet been made. Stöffler (1972) also writes that the crystallographic orientation of the mineral in relation to the shock-front influences which planar structures are formed. For example, (0001)- planar deformation structures in quartz will not develop if the shock front is parallel to (0001).

Sample 54 and 451 contains grains with parallel microstructures that are assumed to depict decorated lamellae (grain 54_10 and 451_28), if interpreted as this, it indicates that some of the grains contain PDFs.

Scenario 2, the described microstructures are PFs
This was the initial expectation and is supported by the "low" pressure range (10-15 GPa) at location 54 and 5, and previous publications where the authors have used the term PFs to describe similar structures (e.g.Cavosie et al. 2010). This original assumption was complicated by the results from the second study where all grains were cast in epoxy and polished to mid-plane for further analysis in SEM. Very few of these grain interiors contained planar microstructures even though PFs were identified on their surfaces. It was possible to identify parallel structures in approx. 5 grains per sample when evaluating the second study (e.g. fig 14); it's unclear whether these are actual PFs. One grain displays distinct fractures that seem to be mended and filled. In his study, Cavosie et al. (2010) describe PFs within some zircons as "conspicuous" parallel to slightly curved fractures.
There is a chance that some of the grains were cut and polished along the PF-planes, but it's highly unlikely that this would be the case for all grains.

Scenario 3, the described microstructures are neither PDFs nor PFs
Since the described microstructures in this study are parallel and in some cases appear in several sets, they are presumed to be a result of an impact-event and could be referred to as parallel microstructures, which is a more vague term to describe similar structures. The formation process of these structures is in this scenario unknown and needs further evaluation. An approximation of the pressure range at the Hättberg location 451 could possibly shed some light on this matter.

The proposal by Erickson et al. (2012) to refer to all planar microstructures in zircon as PFs could potentially be applied, however the general criterion that these fractures also should be visible within the grains must be discarded.

There is also a possibility that some of the microstructures are microtwins. These could be produced along PFs during low pressure (Timms et al 2012).

Based on descriptions of micro twins in zircon by Leroux et al. (1999) & Davis et al. (2011), and the fact that a majority of the grains where angles between grain boundaries were possible to measure turned out to be ~65º, there is a possibility that some PMs are in fact micro twins (Figure 5D and Figure 6E). Since these can develop along PFs at low-pressure ranges (5-20 GPa) it is likely that they would exist in the Siljan samples. Holm et al 2010 observed mechanical Brazil twins in quartz samples from the Siljan impact structure. These occurred mainly outside the central part of the impact structure.

Further studies
It would be interesting to determine the orientations of the parallel microstructures in this study and compare these to earlier findings by Timms et al. (2012) and Leroux et al. (1999). It would also be interesting to investigate if the high-pressure polymorph reidite occurs in any of the zircon samples, for example with X-ray diffraction (XRD). This could support a theory of a possible higher shock-pressure at locations where the zircons contain decorated lamellae, e.g. location 54.

PMs occurring in 65º angles were measured relatively late in this study, with the result that they were not properly investigated. These structures suggest that some PMs might be classified as micro twins. Since the Siljan quartz samples (Holm et al 2010) contained several grains with Brazil twins, this hypothesis should be further looked in to.

Summary of discussion
Several findings of planar microstructures in zircon grains have been discussed. Contradicting views on the nomenclature for shock-metamorphic features in zircon makes it difficult to classify these structures along e.g. quartz, where the nomenclature is well established. Some microstructures found in this study are supposed to be PDFs, based on decorations in the la-

mellae. Other planar lamellae could either be regarded as PFs or PMs. It was not possible to determine crystallographic orientations for the PMs, however, measurements of sets that were facing the camera during the SEM-imaging and had visible c-axis revealed that most of them had sets with boundaries of 65º. This could suggest that these structures are micro-twins. To prove this, the grains would need proper measurements.

9. Conclusions

1. Different types of planar microstructures have been observed in zircon grain samples from the Siljan impact structure. A classification of these structures based on comparisons with previous studies on shock-metamorphosed zircon have been suggested.

2. The found microstructures varied in morphology; the ones that contained decorated lamellae are believed to be PDFs.

3. Few grains contained visible interior PFs.

10. Acknowledgements

I'm very grateful to my supervisors Sanna Holm-Alwmark, Carl Alwmark and Andreas Petersson that have been most helpful during the work on this thesis, both during practical work and for valuable comments on the text! You have all put so much effort into answering questions and giving good advice, thank you!
I would also like to thank my intellectual study partner Wiktor Skoglund for company during the labwork and for all doors you've opened (when my access-card did not work). Finally, I would like to acknowledge Gustaf Holtenäs for guiding me through the physics of shock-waves with great patience and for valuable layout discussions.

11. References

Bischoff, A. & Stoeffler, D., 1992: Shock metamorphism as a fundamental process in the evolution of planetary bodies; information from meteorites: *European Journal of Mineralogy 4*, 707-755.

Bohor, B. F., Betterton, W. J. & Krogh, T. E., 1993: Impact-shocked zircons: discovery of shock-induced textures reflecting increasing degrees of shock metamorphism: *Earth and Planetary Science Letters 119*, 419-424. doi: http://dx.doi.org/10.1016/0012-821X(93)90149-4

Cavosie, A. J., Erickson, T. M. & Timms, N. E., 2015: Nanoscale records of ancient shock deformation: Reidite (ZrSiO4) in sandstone at the Ordovician Rock Elm impact crater: *Geology 43*, 315-318. doi: 10.1130/g36489.1

Cavosie, A. J., Quintero, R. R., Radovan, H. A. & Moser, D. E., 2010: A record of ancient cataclysm in modern sand: Shock microstructures in detrital minerals from the Vaal River, Vredefort Dome, South Africa: *Geological Society of America Bulletin 122*, 1968-1980. doi: 10.1130/B30187.1

Davis, W. J., Moser, D. E., Cupelli, C. L., Barker, I. R., Flowers, R. M., Bowman, J. R., Wooden, J. & Hart, J. R., 2011: New zircon shock phenomena and their use for dating and reconstruction of large impact structures revealed by electron nanobeam (EBSD, CL, EDS) and isotopic U–Pb and (U–Th)/The analysis of the Vredefort dome: *Canadian Journal of Earth Sciences 48*, 117-139. doi: 10.1139/e11-011

Dressler, B. O., Sharpton, V. L. & Schuraytz, B. C., 1998: Shock metamorphism and shock barometry at a complex impact structure: Slate Islands, Canada: *Contrib Mineral Petrol 130*, 275-287.

Engelhardt, W. v. & Bertsch, W., 1969: Shock induced planar deformation structures in quartz from the Ries crater, Germany: *Contributions to Mineralogy and Petrology 20*, 203-234. doi: 10.1007/bf00377477

Erickson, T. M., Cavosie, A. J., Moser, D. E., Barker, I. R. & Radovan, H. A., 2012: Correlating planar microstructures in shocked zircon from the Vredefort Dome at multiple scales: Crystallographic modeling, external and internal imaging, and EBSD structural analysis: *American Mineralogist 98*, 53-65. doi: 10.2138/am.2013.4165

Finch, R. J. & Hanchar, J. M., 2003: Structure and Chemistry of Zircon and Zircon-Group Minerals: *Reviews in Mineralogy and Geochemistry 53*, 1-25.

Forbes, J. W., 2012: *Shock Wave Compression of Condensed Matter*. Dordrecht, Netherlands : Springer Berlin Heidelberg.

French, B. M., 1998: *Traces of Catastrophe: A Handbook of shock-Metamorphic Effects in Terrestrial Meteorite Impact Structures*. Lunar and Planetary Institute, Houston. 120 sid.

Goltrant, O., Cordier, P. & Doukhan, J.-C., 1991: Planar deformation features in shocked quartz; a transmission electron microscopy investigation: *Earth and Planetary Science Letters 106*, 103-115. doi: http://dx.doi.org/10.1016/0012-821X(91)90066-Q

Goltrant, O., Leroux, H., Doukhan, J.-C. & Cordier, P., 1992: Formation mechanisms of planar deformation features in naturally shocked quartz: *Physics of the Earth and Planetary Interiors 74*, 219-240. doi: http://dx.doi.org/10.1016/0031-9201(92)90012-K

Harley, S. L., Kelly, N. M. & MöLler, A., 2007: Zircon Behaviour and the Thermal Histories of Mountain Chains: *Elements 3*, 25-30.

Holm, S., Alwmark, C., Alvarez, W. & Schmitz, B., 2011: Shock barometry of the Siljan impact structure, Sweden: *Meteoritics & Planetary Science 46*, 1888-1909. doi: 10.1111/j.1945-5100.2011.01303.x

Hoskin, P. W. O. & Schaltegger, U., 2003: The Composition of Zircon and Igneous and Metamorphic Petrogenesis: *Reviews in Mineralogy and Geochemistry 53*, 27-62. doi: 10.2113/0530027

Jourdan, F. & Reimold, W. U., 2012: Age of the Siljan Impact Structure (abstract). *75th Annual Meeting Meteoritical Society.* Cairns, abstract # 5093 1s.

Kusaba, K., Syono, Y., Kikuchi, M. & Fukuoka, K., 1985: Shock behavior of zircon; phase transition to scheelite structure and decomposition: *Earth and Planetary Science Letters 72*, 433-439.

Langenhorst, F., 2002: Shock metamorphism of some minerals: Basic introduction and microstructural observations: *Bulletin of the Czech Geological Survey 77*, 265–282.

Leroux, H., Reimold, W. U., Koeberl, C., Hornemann, U. & Doukhan, J. C., 1999: Experimental shock deformation in zircon: a transmission electron microscopic study: *Earth and Planetary Science Letters 169*, 291-301. doi: http://dx.doi.org/10.1016/S0012-821X(99)00082-5

Reid, A. F. & Ringwood, A. E., 1969: Newly observed high pressure transformations in Mn3O4, CaAl2O4, and ZrSiO4: *Earth and Planetary Science Letters 6*, 205-208. doi: http://dx.doi.org/10.1016/0012-821X(69)90091-0

Sharp, T. G. & Decarli, P. S., 2006: *Shock Effects in Meteorites*. Tuscon, University of Arizona press.

Stöffler, D., 1972: Deformation and transformation of rock-forming minerals by natural and experimental shock processes: I. Behaviour of minerals under shock-compression.: *Fortschritte der Mineralogie 49*, 50-113.

Stöffler, D. & Langenhorst, F., 1994: Shock metamorphism of quartz in nature and experiment: I. Basic observation and theory*: *Meteoritics 29*, 155-181. doi: 10.1111/j.1945-5100.1994.tb00670.x

Svahn, F. 2014. *Traces of impact in crystalline rock.* (Bachelor's thesis), Lund University.

Timms, N. E. & Healy, D., 2013: *The Effects of Anisotropic Elastic Properties on Shock Deformation Microstructures in Zircon and Quartz*. LPI, The Woodlands, Texas. 1862 pp

Timms, N. E., Reddy, S. M., Healy, D., Nemchin, A. A., Grange, M. L., Pidgeon, R. T. & Hart, R., 2012: Resolution of impact-related microstructures in lunar zircon: A shock-deformation mechanism map: *Meteoritics & Planetary Science 47*, 120-141. doi: 10.1111/j.1945-5100.2011.01316.x

Ulf Söderlund & Johansson, L., 2002: A simple way to extract baddeleyite (ZrO2): *Geochem. Geophys. Geosyst. 3*, 7. doi: 10.1029/2001GC000212

Wittmann, A., Kenkmann, T., Schmitt, R. T. & Stöffler, D., 2006: Shock-metamorphosed zircon in terrestrial impact craters: *Meteoritics & Planetary Science 41*, 433-454. doi: 10.1111/j.1945-5100.2006.tb00472.x

12. Appendix A

SEM-images of mid-sections (polished grains)

Sample 451

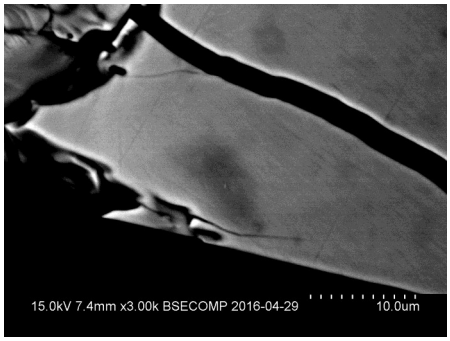

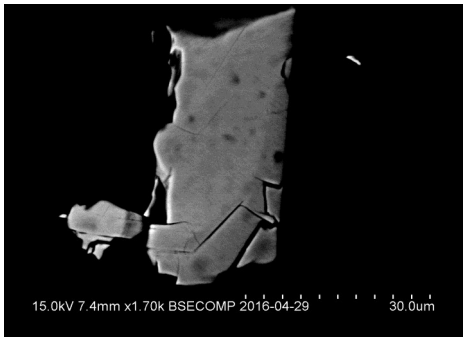

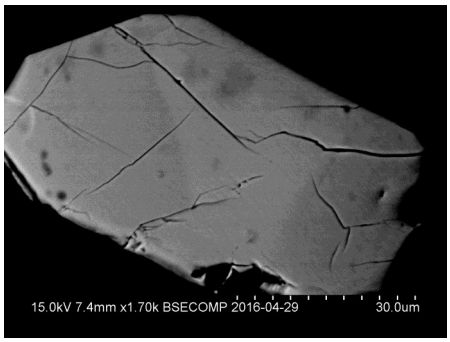

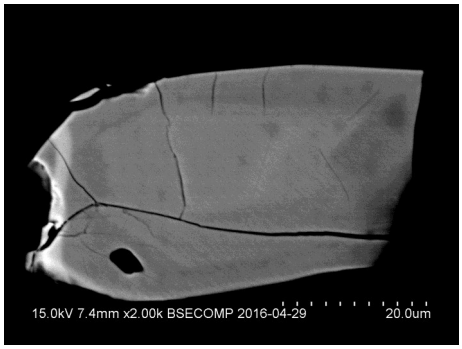

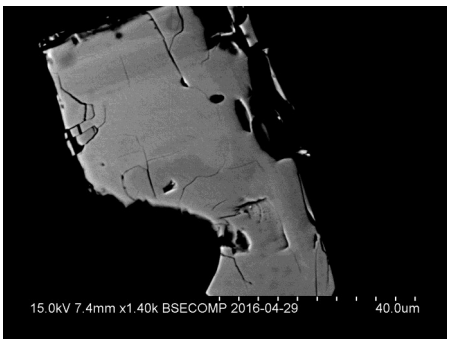

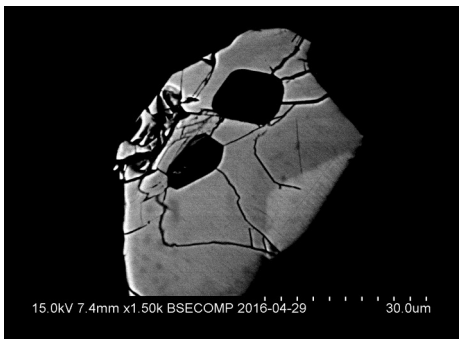

Sample 5

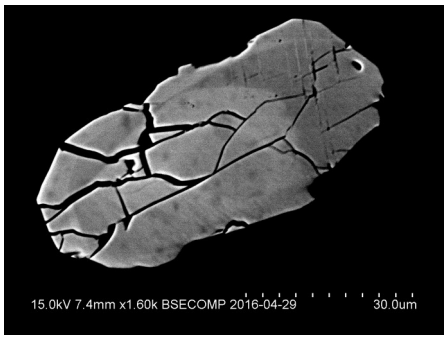

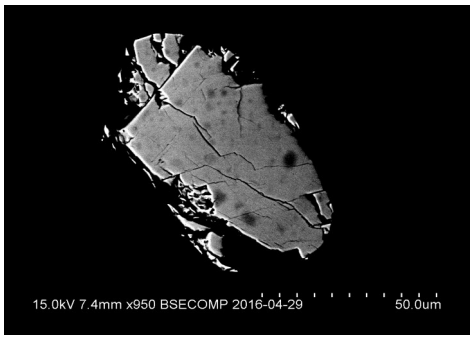

Sample 54

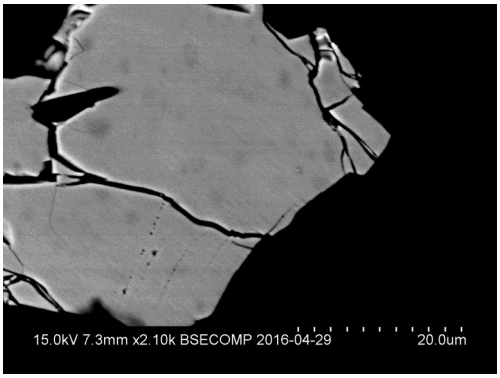
15.0kV 7.3mm x2.10k BSECOMP 2016-04-29
20.0um

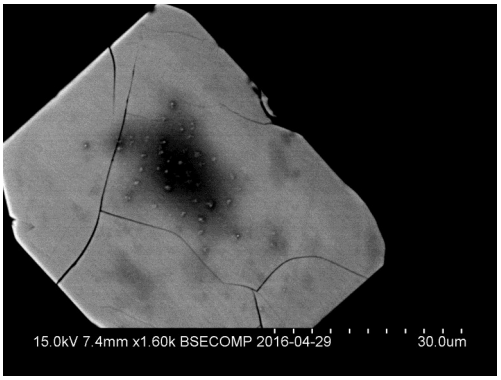
15.0kV 7.4mm x1.60k BSECOMP 2016-04-29
30.0um

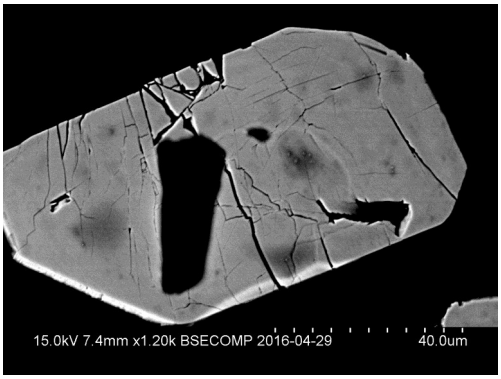
15.0kV 7.4mm x1.20k BSECOMP 2016-04-29
40.0um

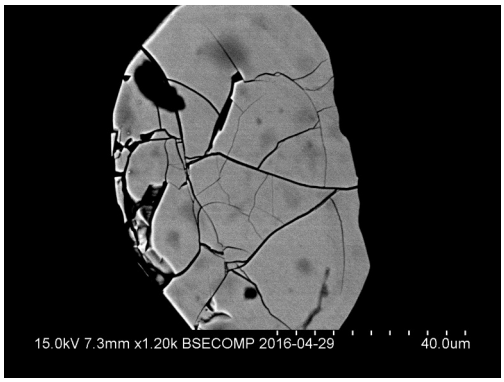
15.0kV 7.3mm x1.20k BSECOMP 2016-04-29
40.0um

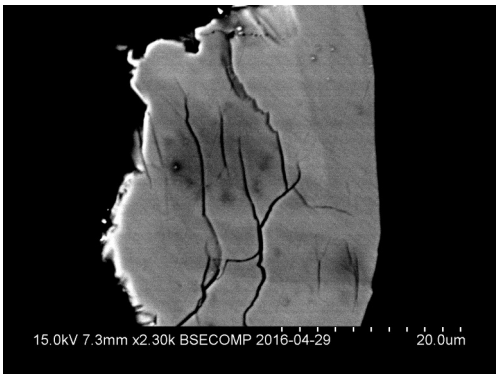
15.0kV 7.3mm x2.30k BSECOMP 2016-04-29
20.0um

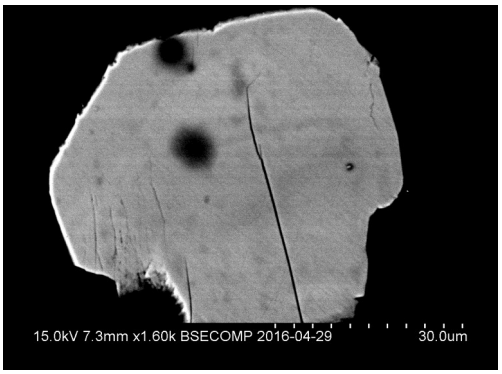
15.0kV 7.3mm x1.60k BSECOMP 2016-04-29
30.0um

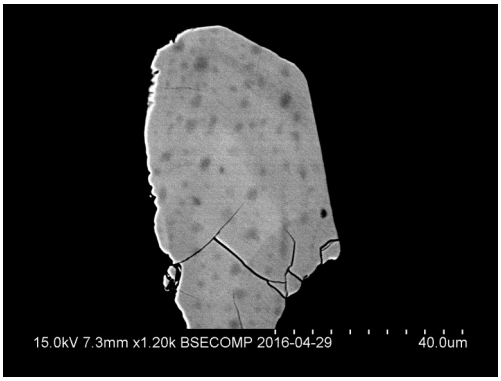
15.0kV 7.3mm x1.20k BSECOMP 2016-04-29
40.0um

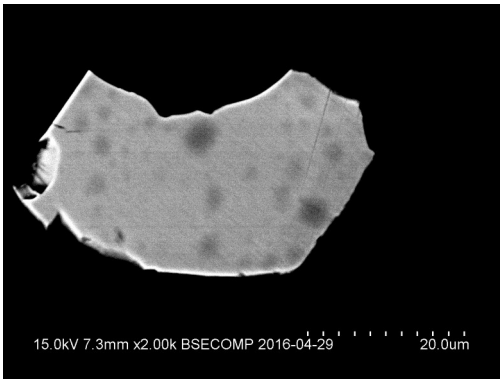
15.0kV 7.3mm x2.00k BSECOMP 2016-04-29
20.0um

SEM-images from sample 54

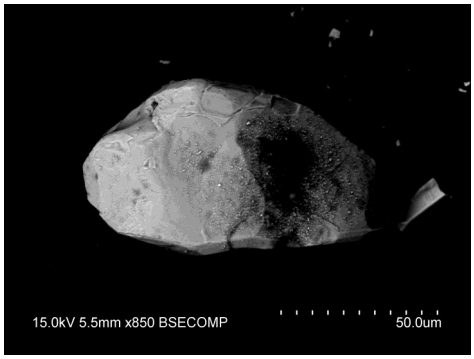

Sample 54_2

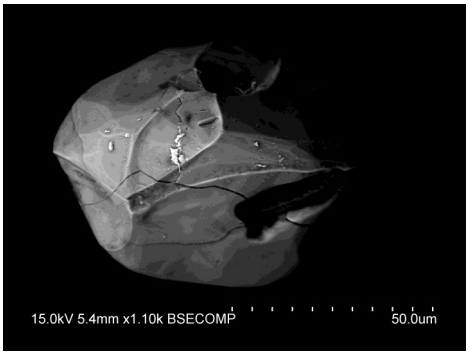

Sample 54_3 Rounded grain, no visible PMs. One major fracture going from right to left. Vain-like structures.

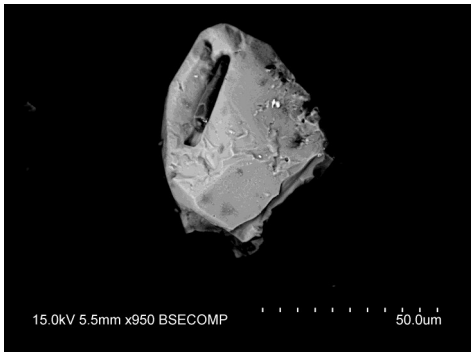

Sample 54_4 No visible PMs

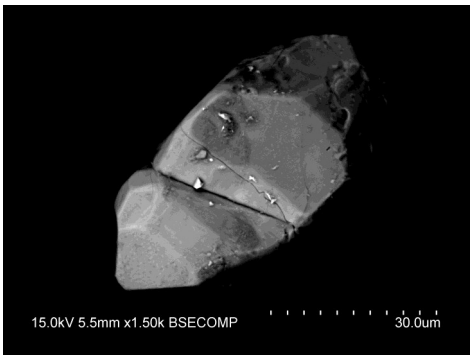

Sample 54_5 Relatively euhedral crystal. Distinct "fracture" perpendicular to c-axis.

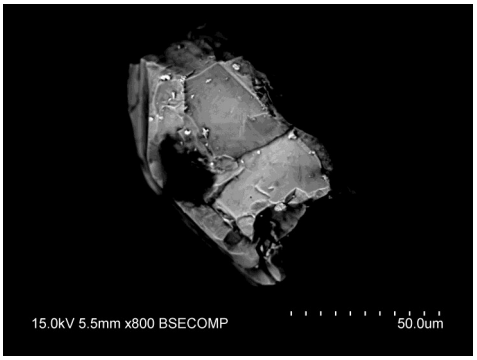

Sample 54_7 Linear marks, light in colour, in several directions.

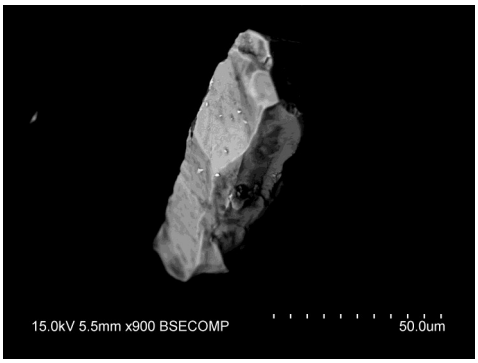

Sample 54_8

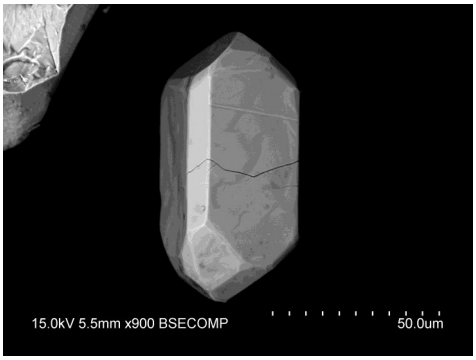

Sample 54_9 Euhedral crystal shape, one major fracture ranging from left to right.

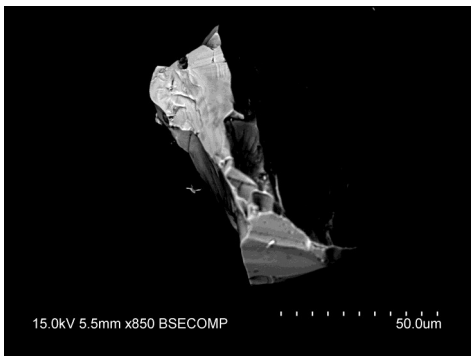

Sample 54_12

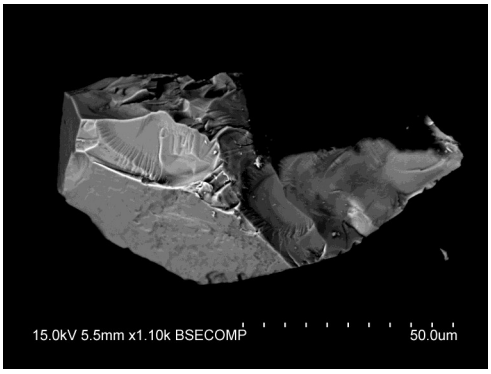

Sample 54_13

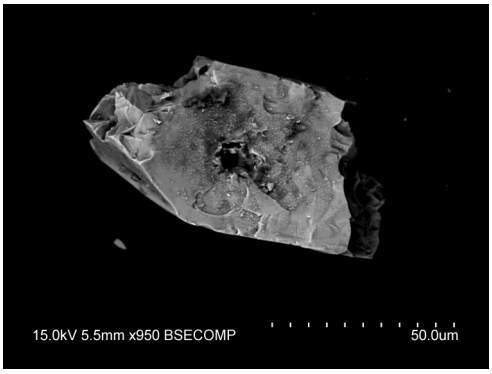

Sample 54_15 Black dust covering the surface. No visible PMs.

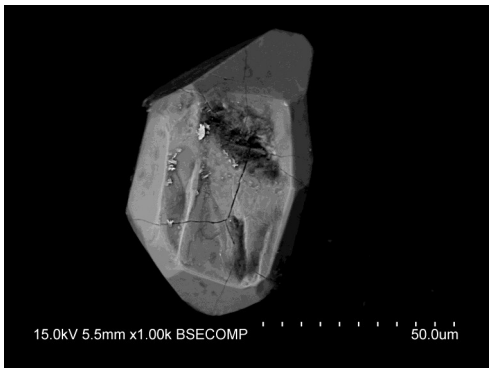

Sample 54_16 No visible PMs. Relatively euhedral.

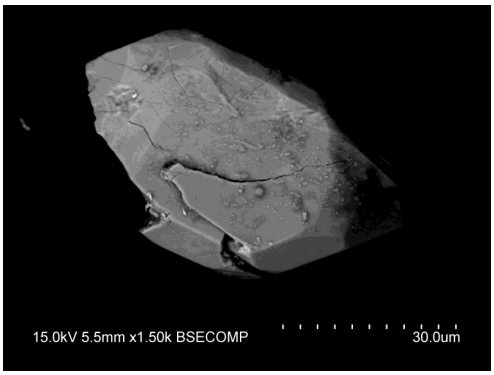

Sample 54_17 Several small fractures in various orientations.

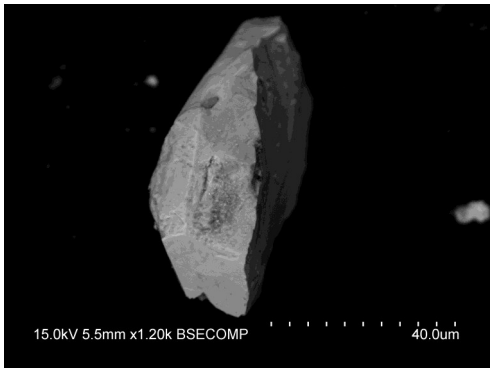

Sample 54_18

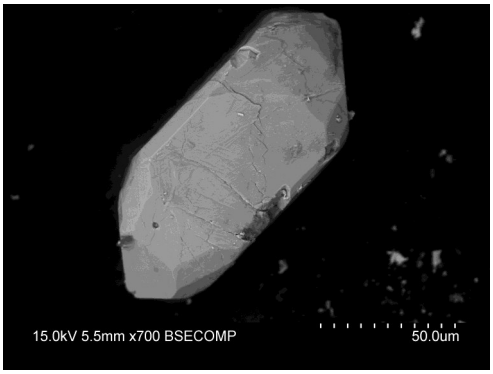

Sample 54_19 Lineation at the surface. At least one set of PMs, possibly more.

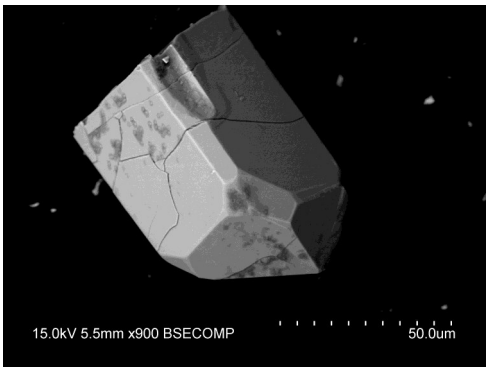

Sample 54_20

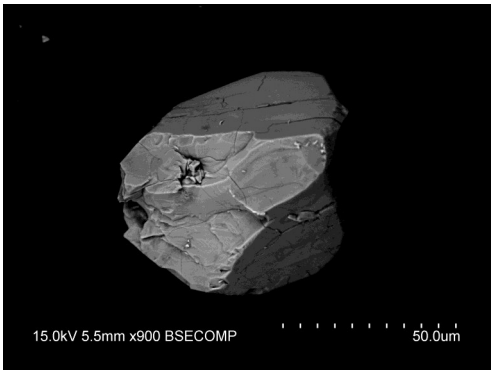

Sample 54_21 Rounded grain. Large parallel fractures at upper half. Fractures in various orientations covering surface.

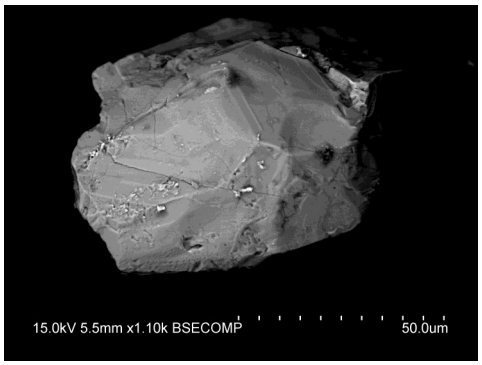

Sample 54_22
Rounded fragment with a rough surface. Light streaks in the center.

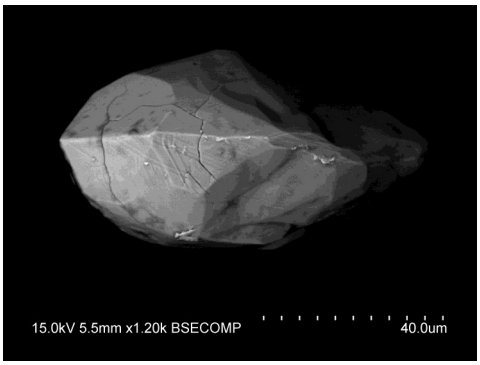

Sample 54_23

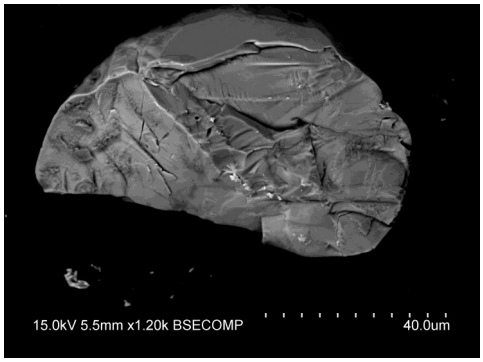

Sample 54_24

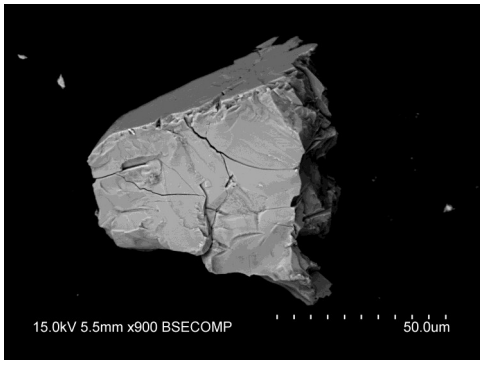

Sample 54_25

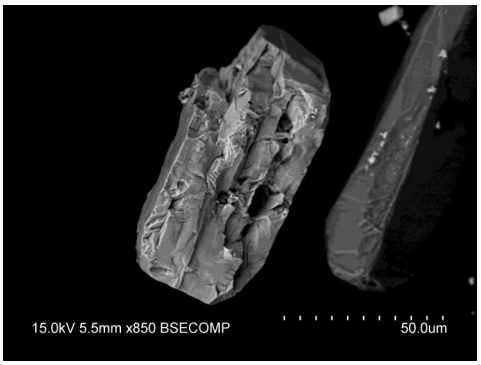

Sample 54_26

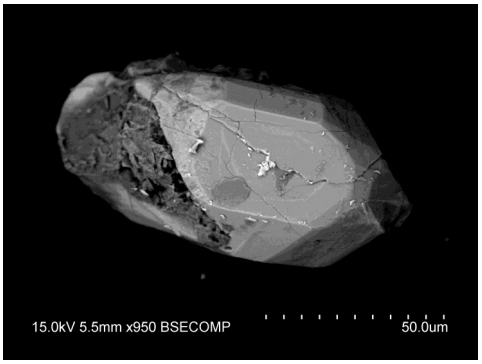

Sample 54_27
Relatively euhedral crystal, left part damaged. Several fractures and signs of zoning

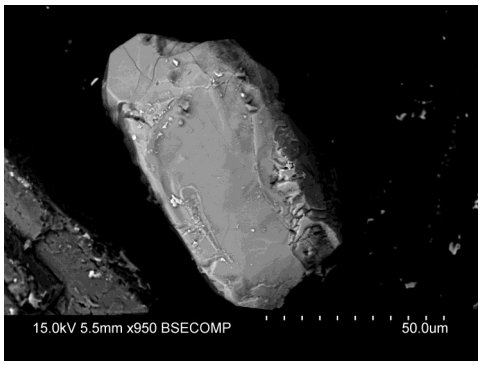

Sample 54_28

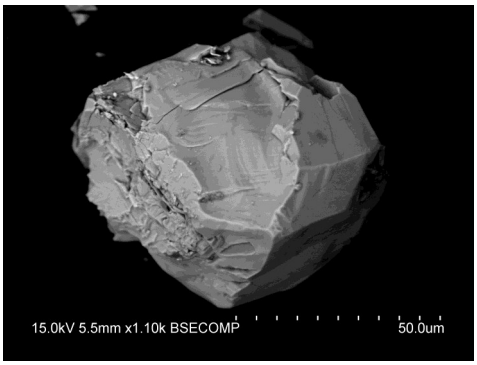

Sample 54_29
Snowball shaped. No distinct c-axis. Several fractures in various orientations, some of them possibly conchoidal fractures.

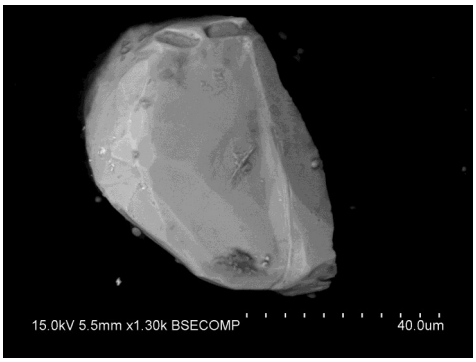

Sample 54_32

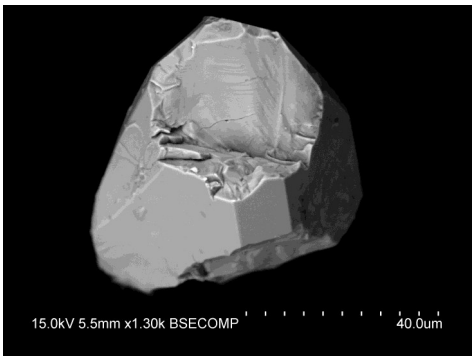

Sample 54_33

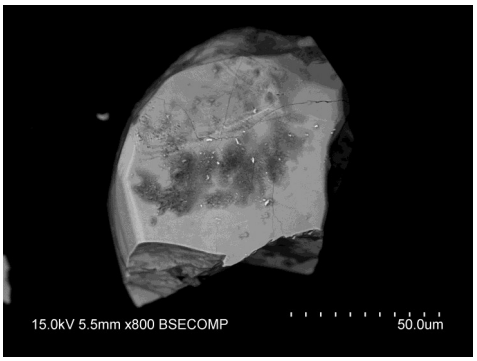

Sample 54_34
Potential PMs visible at far left corner of the grain fragment.
Dusty surface, some minor fractures.

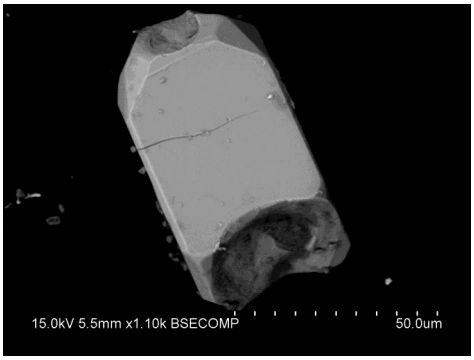

Sample 54_35
Relatively euhedral crystal. No visible PFs, one larger fracture perpendicular to c-axis

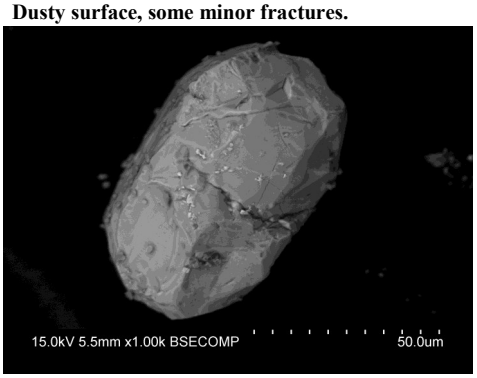

Sample 54_36

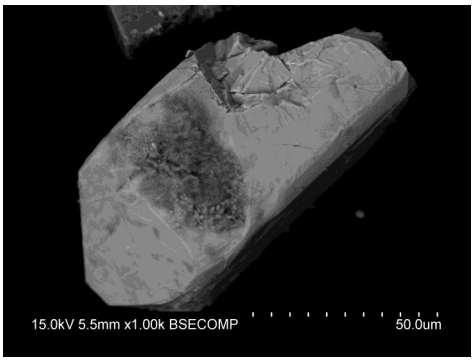

Sample 54_37

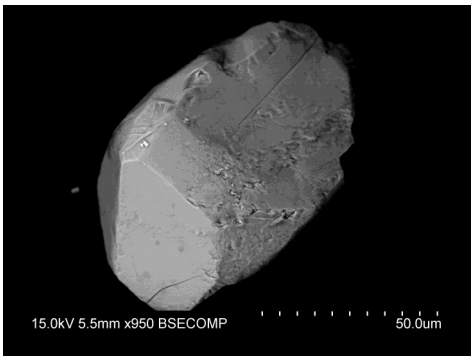

Sample 54_38

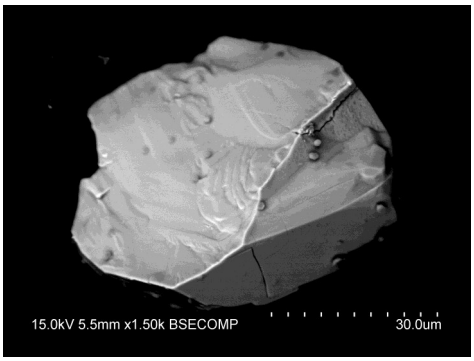

Sample 54_39

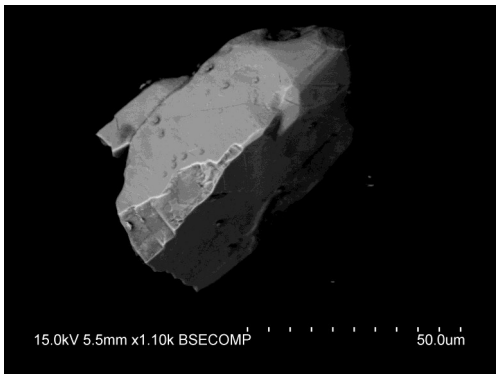

Sample 54_41

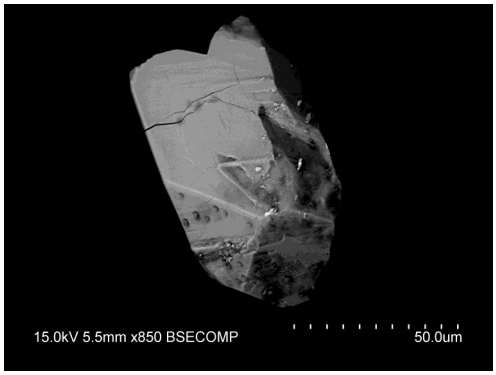

Sample 54_42

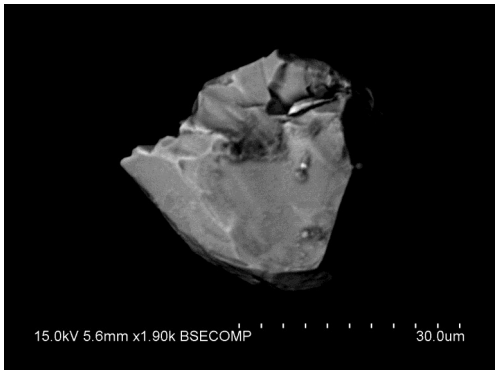

Sample 54_43
Poor resolution. Not possible to establish any surface structures.

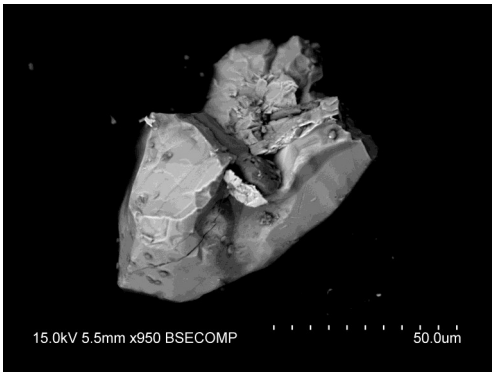

Sample 54_44

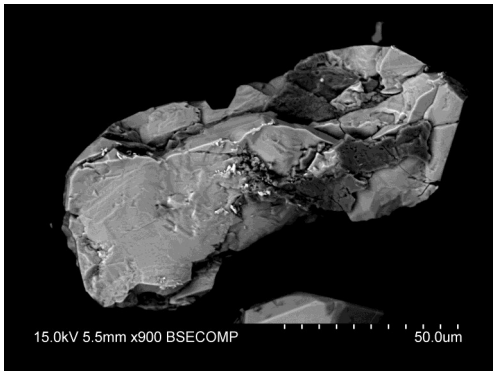

Sample 54_45

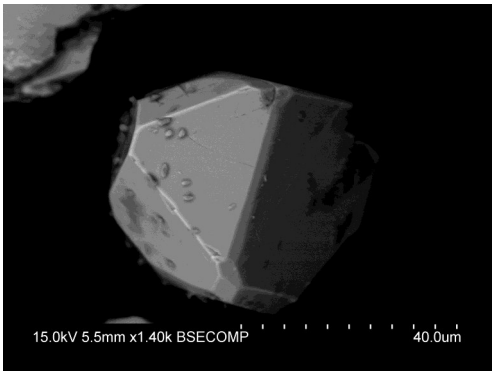

Sample 54_46

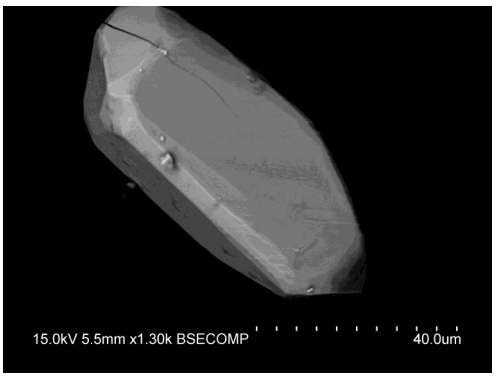

Sample 54_47
Euhedral crystal. Few fractures, one ranging along c-axis.

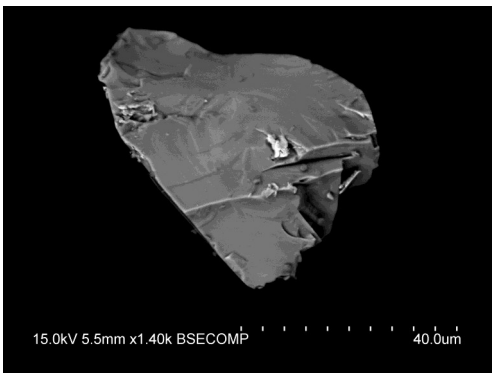

Sample 54_49
Exposed interior of grain. No visible PMs

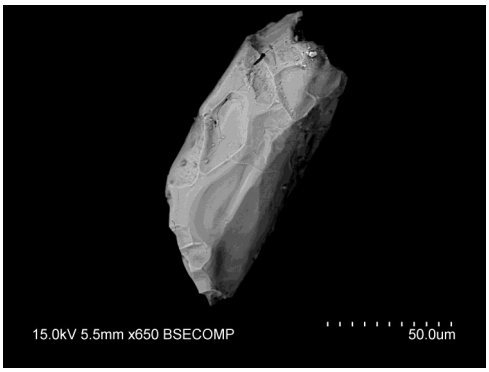

Sample 54_50

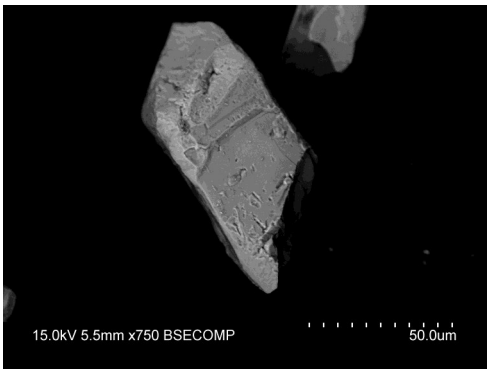

Sample 54_51
"Pinch-marks" all over grain surface.

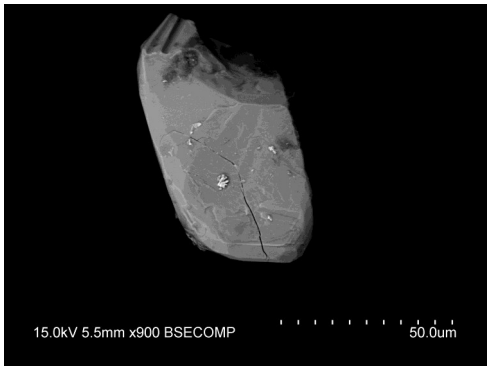

Sample 54_52

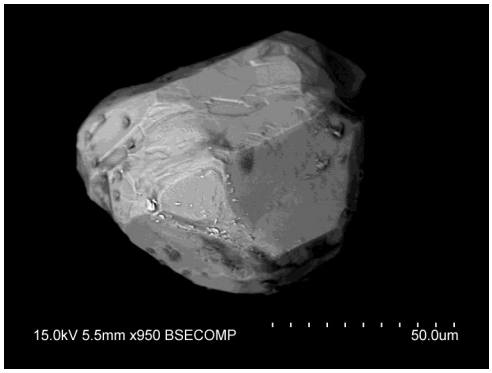

Sample 54_53

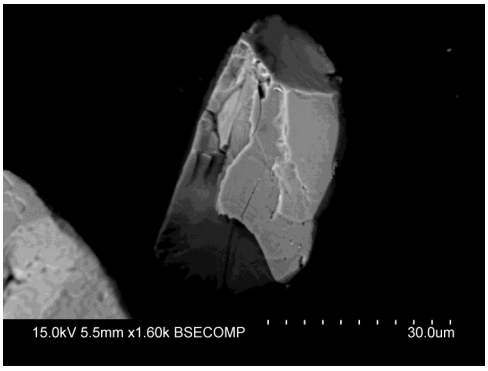

Sample 54_54

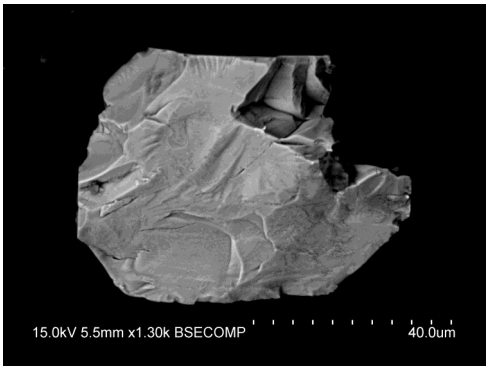

Sample 54_55

SEM-images of sample 5

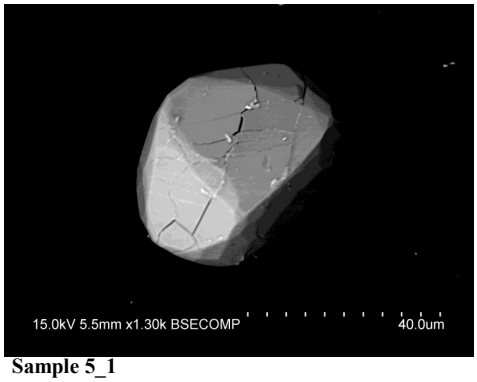

Sample 5_1

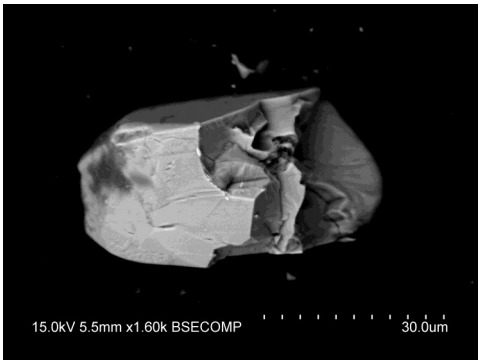

Sample 5_2

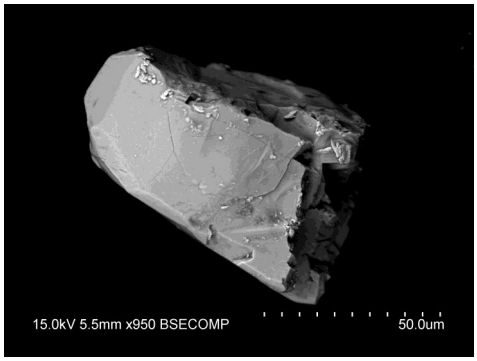

Sample 5_3

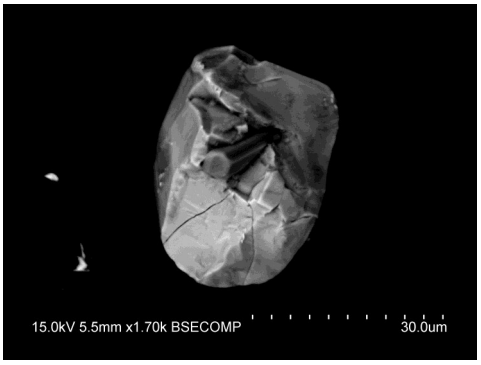

Sample 5_5
Dark inclusion

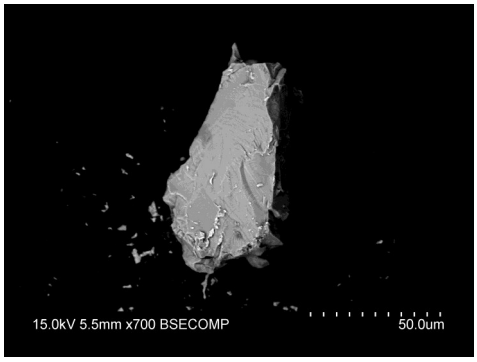

Sample 5_6

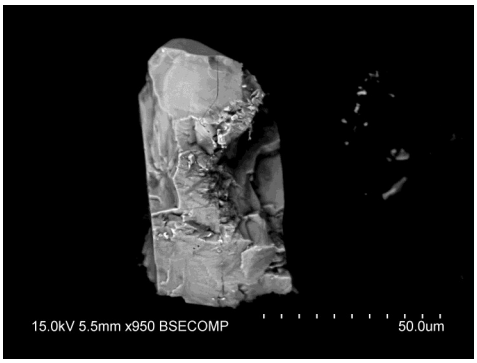

Sample 5_7
Very fractured surface, no visible PMs

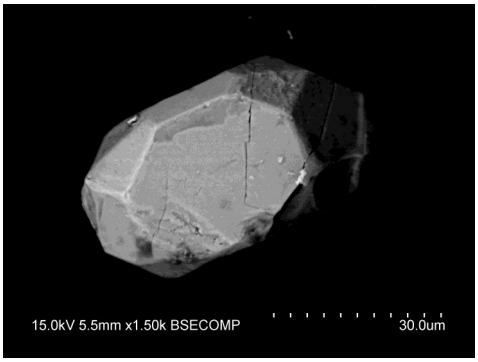

Sample 5_8
Small, relatively euhedral grain

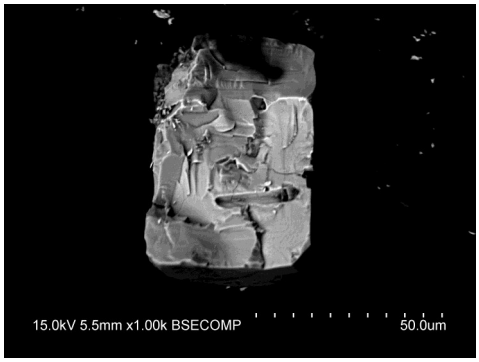

Sample 5_9

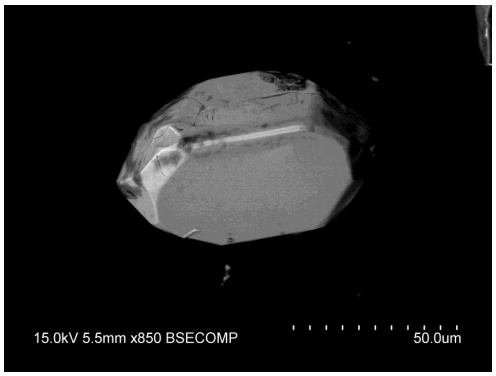

Sample 5_10

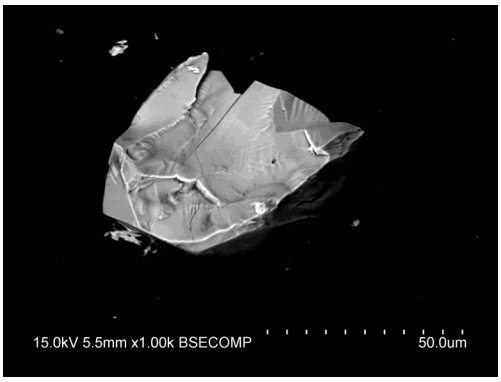

Sample 5_11

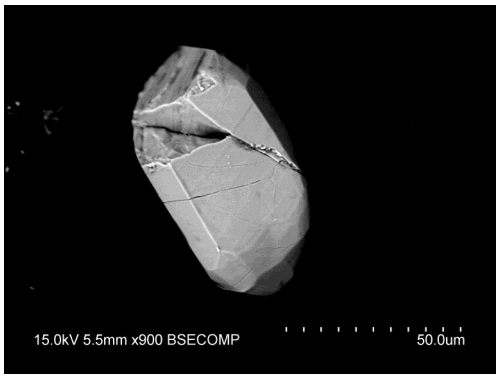

Sample 5_12

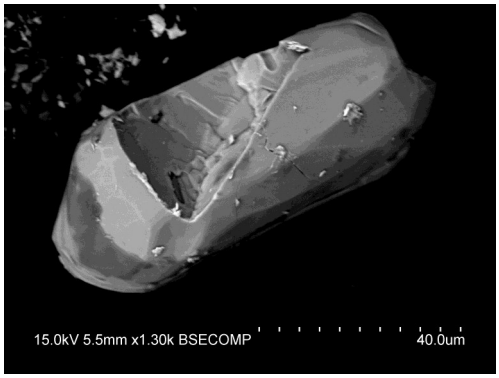

Sample 5_14

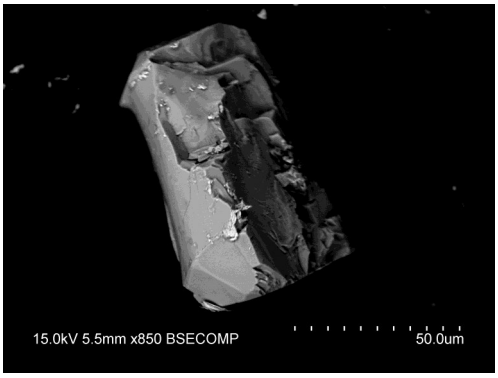

Sample 5_16
PMs almost perpendicular to c-axis

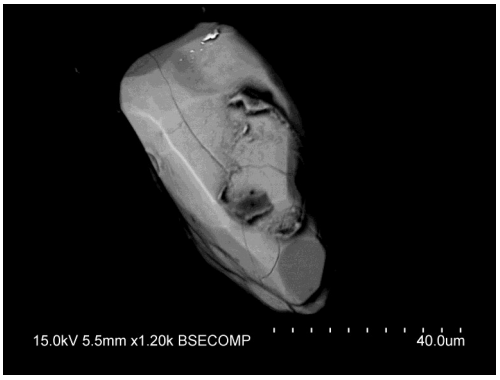

Sample 5_17

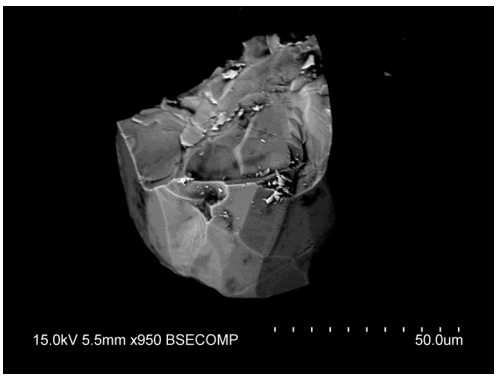

Sample 5_18

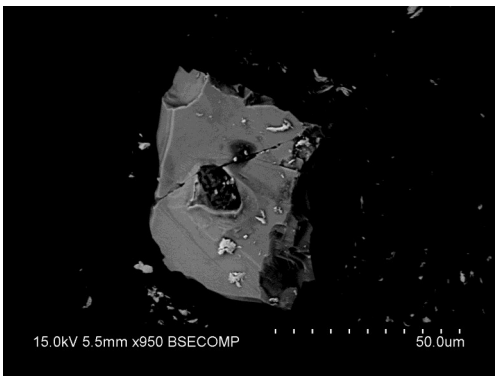

Sample 5_19

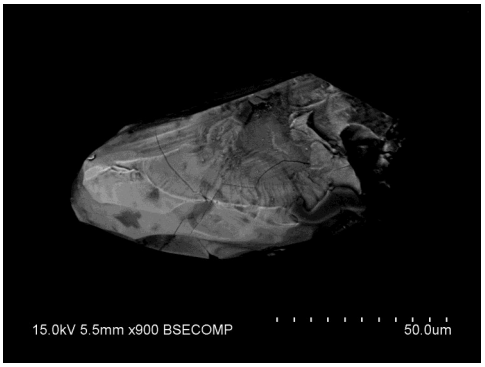

Sample 5_20

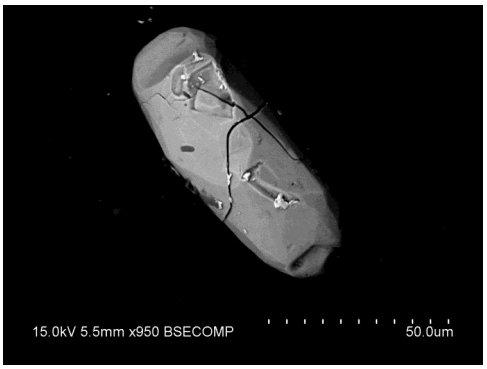

Sample 5_21

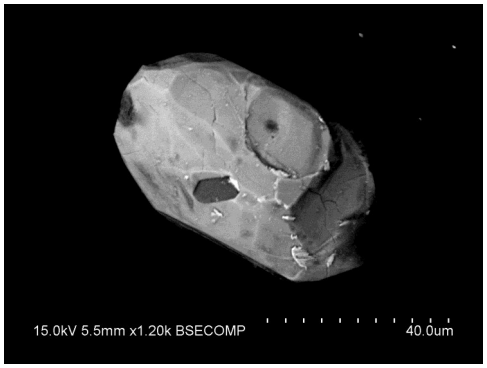

Sample 5_22

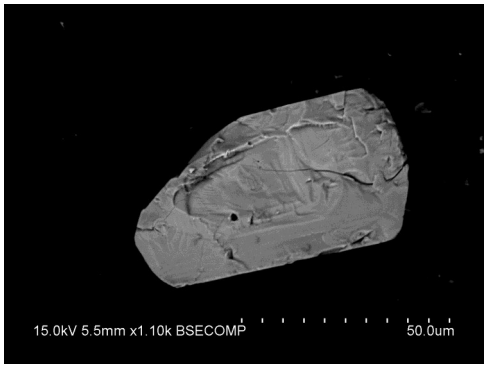

Sample 5_23
Image shows interior zoning. No visible PMs

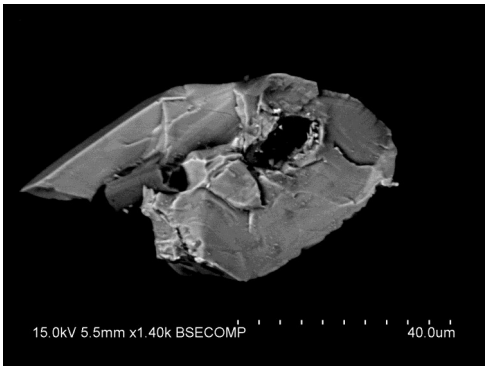

Sample 5_24

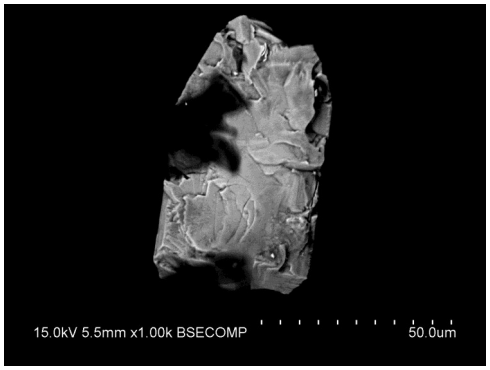

Sample 5_25

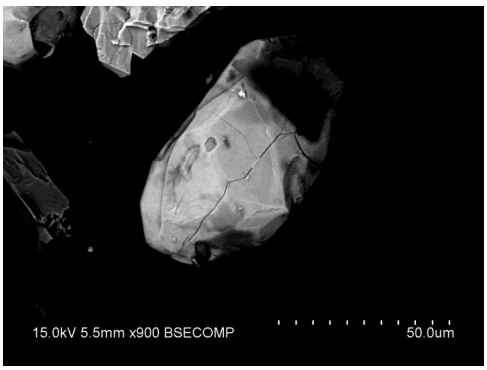

Sample 5_26
Some major fractures but no PMs. Dust covering 1/3 of surface.

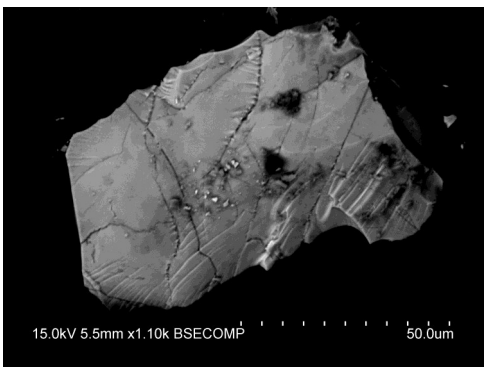

Sample 5_27
Distinct striation, somewhat curved. Possibly conchoidal fractures.

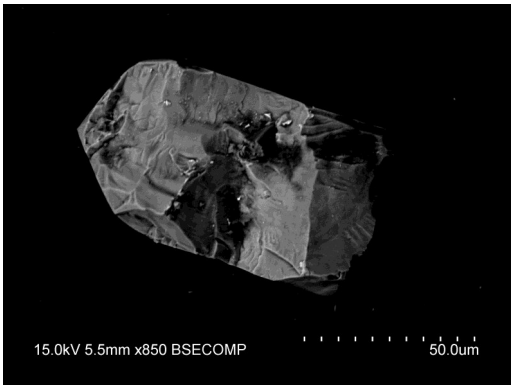

Sample 5_28

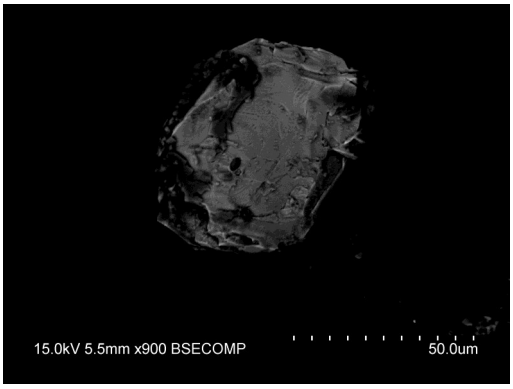

Sample 5_29

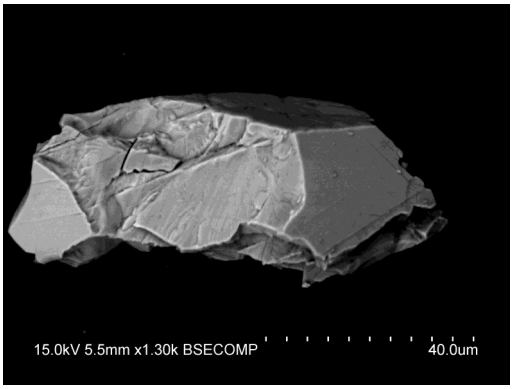

Sample 5_32 Possibly two sets of PMs.

SEM-images from sample 451

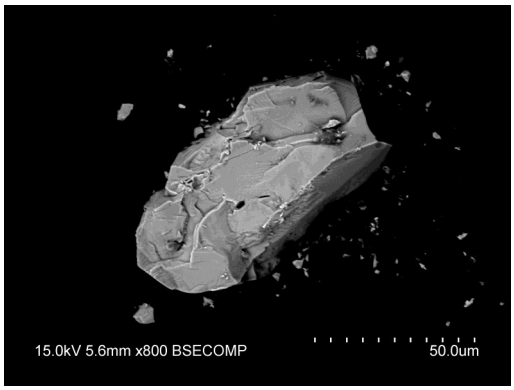

Sample 451_1

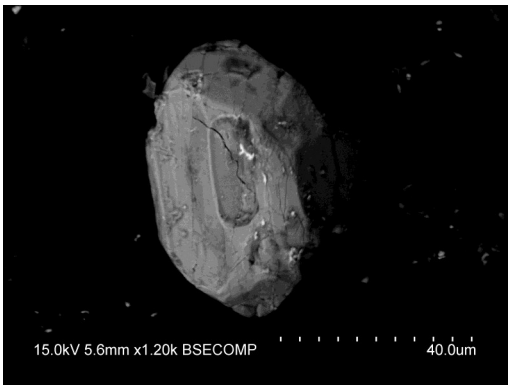

Sample 451_2
Several fractures aligning with c-axis.

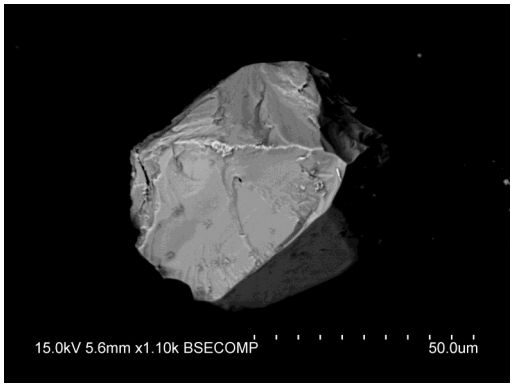

Sample 451_3

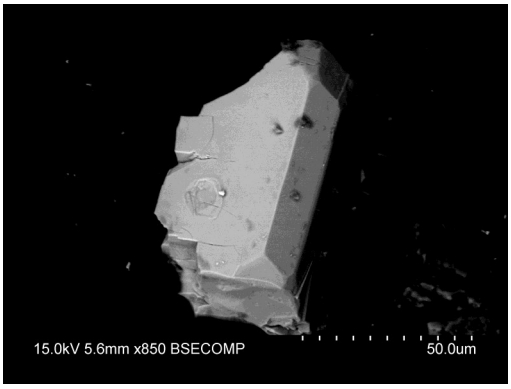

Sample 451_4

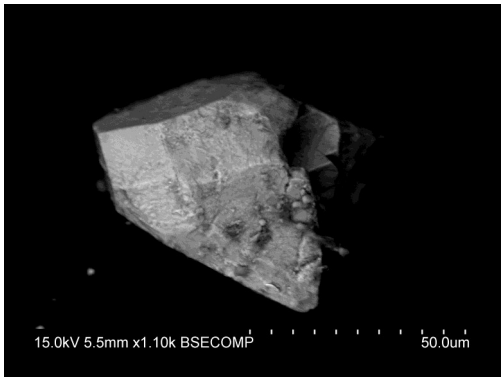

Sample 451_5

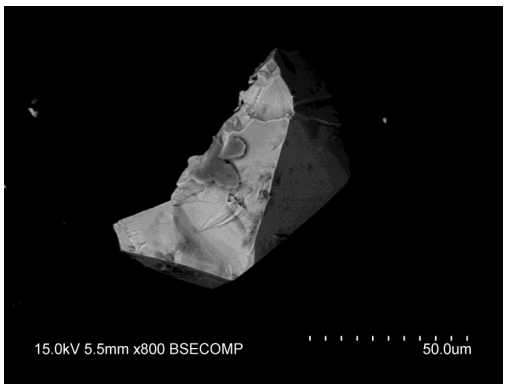

Sample 451_6

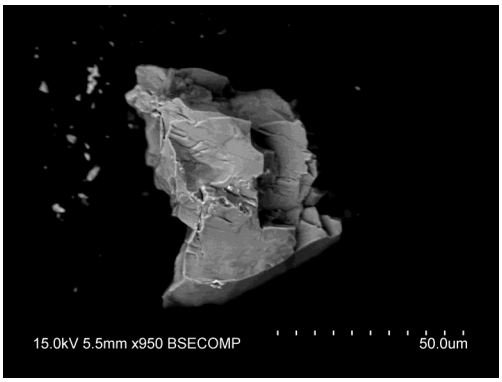

Sample 451_7

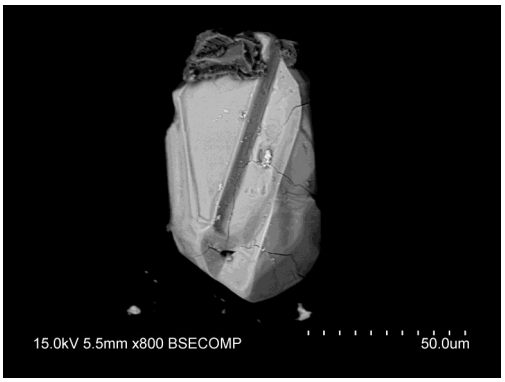

Sample 451_8

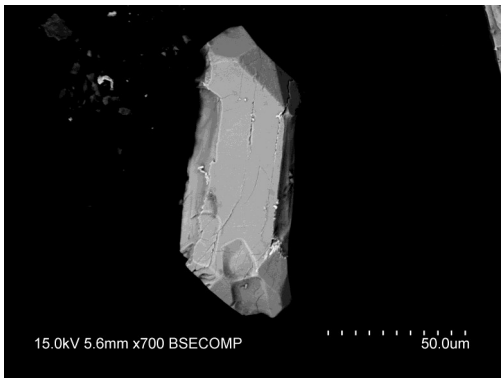

Sample 451_9 Several small fractures

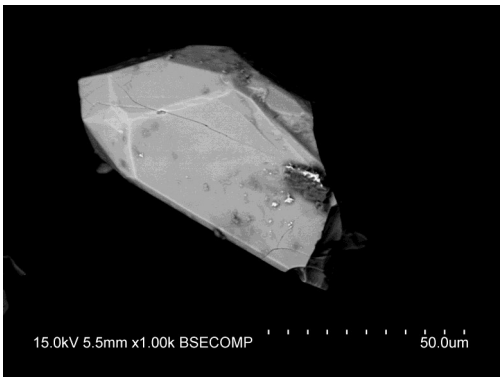

Sample 451_10

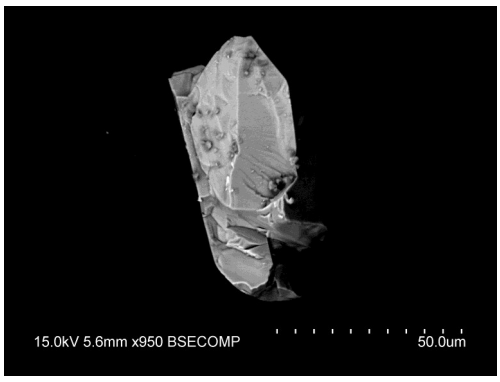

Sample 451_11

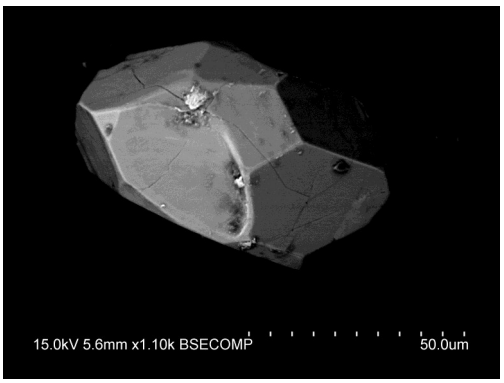

Sample 451_12

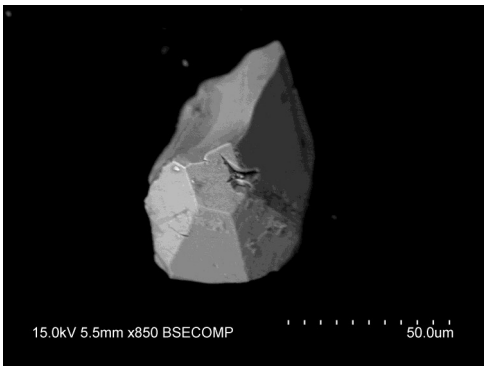

Sample 451_13

Sample 451_14

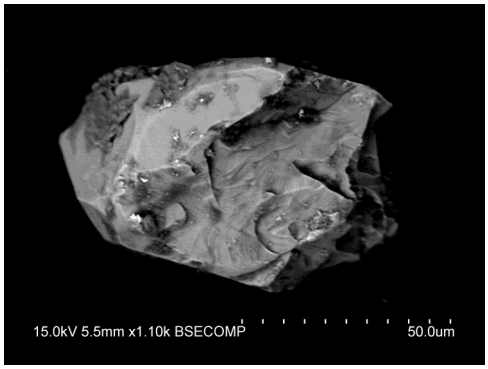

Sample 451_15

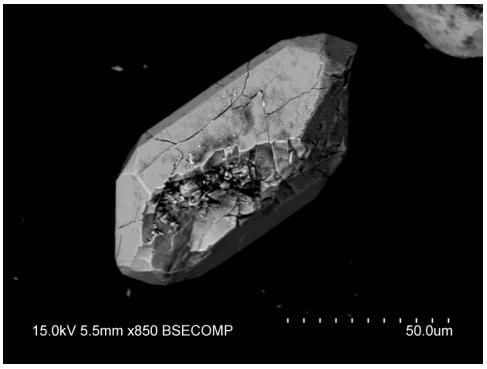

Sample 451_16

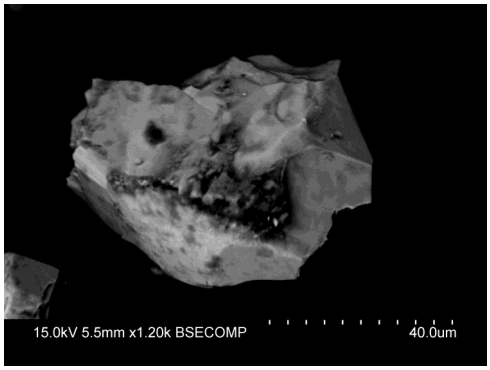

Sample 451_17

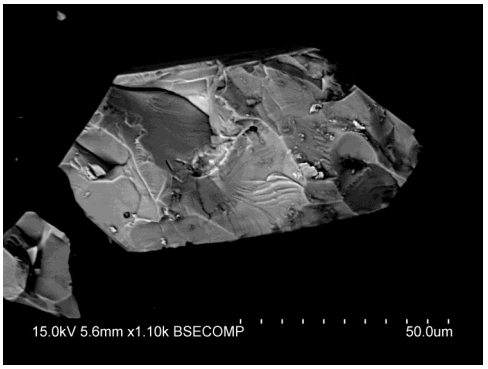

Sample 451_19

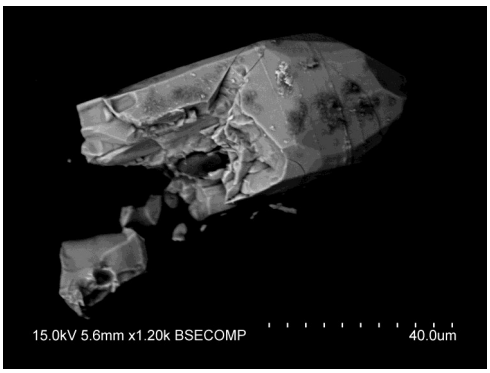

Sample 451_20. PMs perpendicular to c-axis.

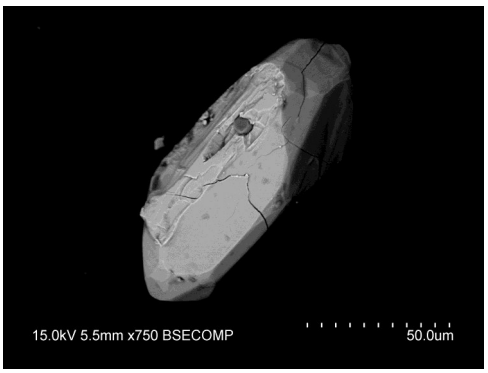

Sample 451_21

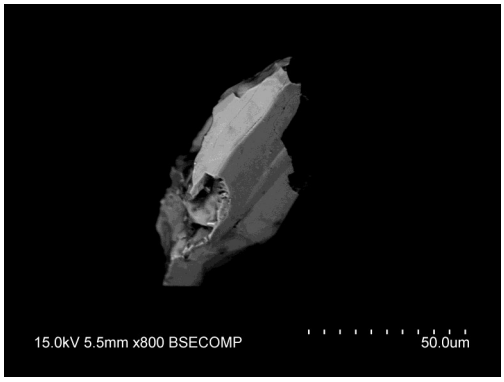

Sample 451_22

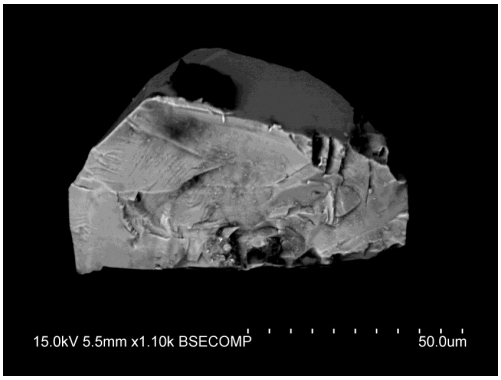

Sample 451_23

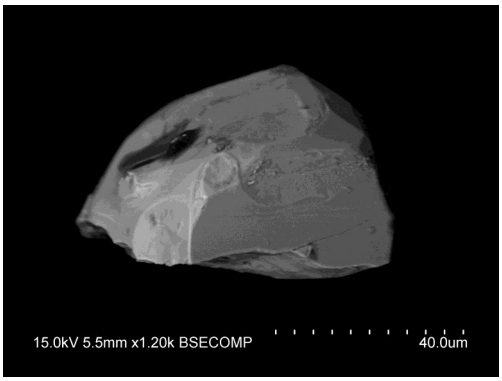

Sample 451_24

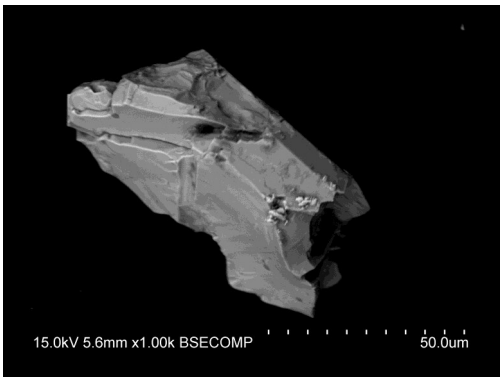

Sample 451_25

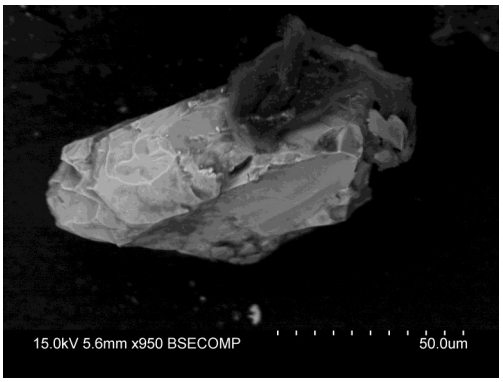

Sample 451_26

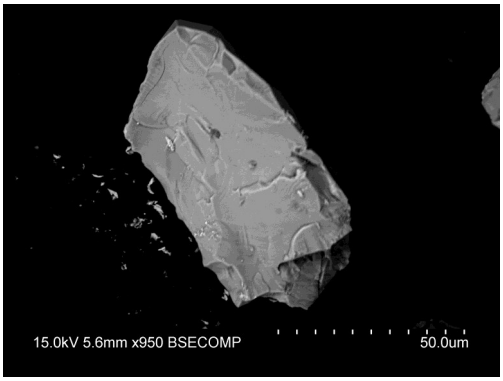

Sample 451_27

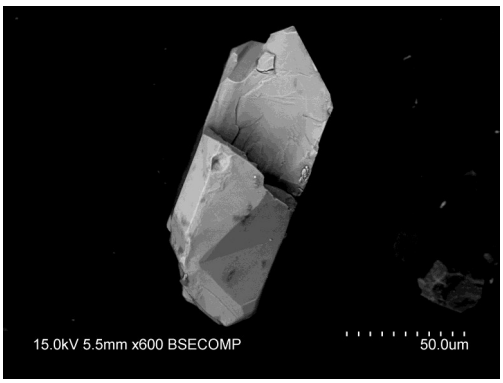

Sample 451_29

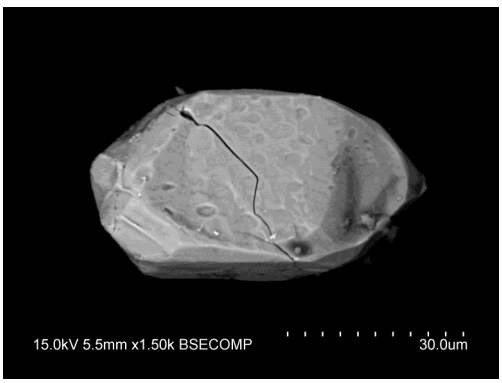

Sample 451_30

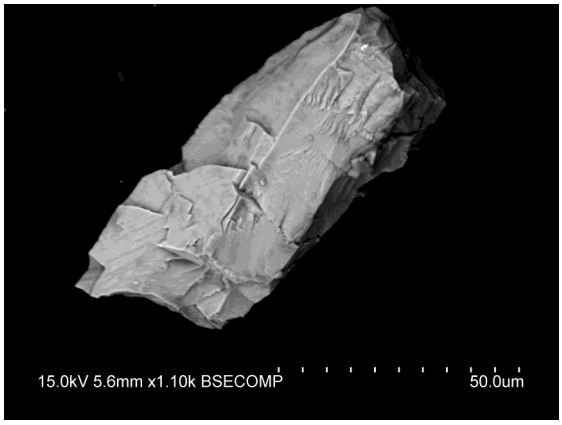

Sample 451_31

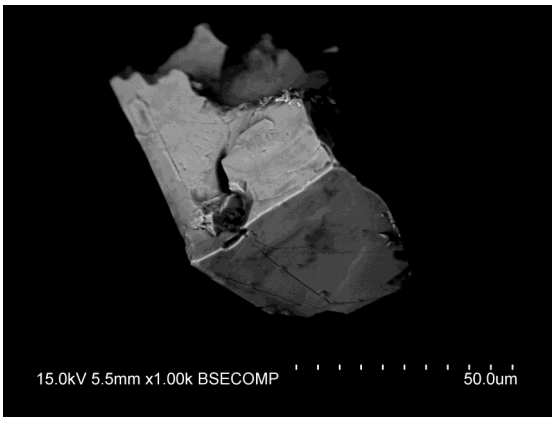

Sample 451_32

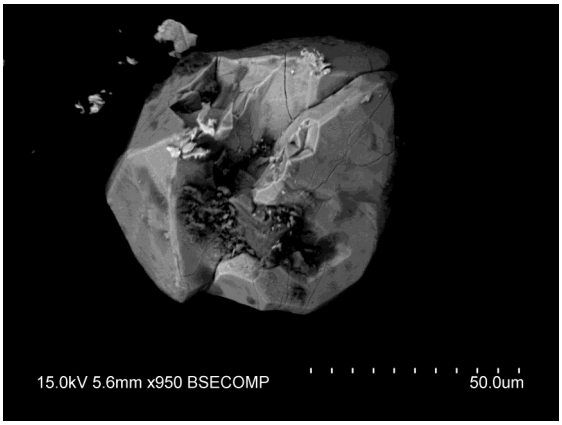

Sample 451_33

Tidigare skrifter i serien ”Examensarbeten i Geologi vid Lunds universitet”:

431. Landgren, Susanne, 2015: Using calcein-filled osmotic pumps to study the calcification response of benthic foraminifera to induced hypoxia under *in situ* conditions: An experimental approach. (45 hp)
432. von Knorring, Robert, 2015: Undersökning av karstvittring inom Kristianstadsslättens NV randområde och bedömning av dess betydelse för grundvattnets sårbarhet. (30 hp)
433. Rezvani, Azadeh, 2015: Spectral Time Domain Induced Polarization - Factors Affecting Spectral Data Information Content and Applicability to Geological Characterization. (45 hp)
434. Vasilica, Alexander, 2015: Geofysisk karaktärisering av de ordoviciska kalkstensenheterna på södra Gotland. (15 hp)
435. Olsson, Sofia, 2015: Naturlig nedbrytning av klorerade lösningsmedel: en modellering i Biochlor baserat på en fallstudie. (15 hp)
436. Huitema, Moa, 2015: Inventering av föroreningar vid en brandövningsplats i Linköpings kommun. (15 hp)
437. Nordlander, Lina, 2015: Borrningsteknikens påverkan vid provtagning inför dimensionering av formationsfilter. (15 hp)
438. Fennvik, Erik, 2015: Resistivitet och IP-mätningar vid Äspö Hard Rock Laboratory. (15 hp)
439. Pettersson, Johan, 2015: Paleoekologisk undersökning av Triberga mosse, sydöstra Öland. (15 hp)
440. Larsson, Alfred, 2015: Mantelplymer - realitet eller *ad hoc*? (15 hp)
441. Holm, Julia, 2015: Markskador inom skogsbruket - jordartens betydelse (15 hp)
442. Åkesson, Sofia, 2015: The application of resistivity and IP-measurements as investigation tools at contaminated sites - A case study from Kv Renen 13, Varberg, SW Sweden. (45 hp)
443. Lönsjö, Emma, 2015: Utbredningen av PFOS i Sverige och världen med fokus på grundvattnet – en litteraturstudie. (15 hp)
444. Asani, Besnik, 2015: A geophysical study of a drumlin in the Åsnen area, Småland, south Sweden. (15 hp)
445. Ohlin, Jeanette, 2015: Riskanalys över pesticidförekomst i enskilda brunnar i Sjöbo kommun. (15 hp)
446. Stevic, Marijana, 2015: Identification and environmental interpretation of microtextures on quartz grains from aeolian sediments - Brattforsheden and Vittskövle, Sweden. (15 hp)
447. Johansson, Ida, 2015: Is there an influence of solar activity on the North Atlantic Oscillation? A literature study of the forcing factors behind the North Atlantic Oscillation. (15 hp)
448. Halling, Jenny, 2015: Inventering av sprickmineraliseringar i en del av Sorgenfrei-Tornquistzonen, Dalby stenbrott, Skåne. (15 hp)
449. Nordas, Johan, 2015: A palynological study across the Ordovician Kinnekulle. (15 hp)
450. Åhlén, Alexandra, 2015: Carbonatites at the Alnö complex, Sweden and along the East African Rift: a literature review. (15 hp)
451. Andersson, Klara, 2015: Undersökning av slugtestsmetodik. (15 hp)
452. Ivarsson, Filip, 2015: Hur bildades Bushveldkomplexet? (15 hp)
453. Glommé, Alexandra, 2015: $^{87}Sr/^{86}Sr$ in plagioclase, evidence for a crustal origin of the Hakefjorden Complex, SW Sweden. (45 hp)
454. Kullberg, Sara, 2015: Using Fe-Ti oxides and trace element analysis to determine crystallization sequence of an anorthosite-norite intrusion, Älgön SW Sweden. (45 hp)
455. Gustafsson, Jon, 2015: När började plattektoniken? Bevis för plattektoniska processer i geologisk tid. (15 hp)
456. Bergqvist, Martina, 2015: Kan Ölands grundvatten öka vid en uppdämning av de utgrävda dikena genom strandvallarna på Ölands östkust? (15 hp)
457. Larsson, Emilie, 2015: U-Pb baddeleyite dating of intrusions in the southeasternmost Kaapvaal Craton (South Africa): revealing multiple events of dyke emplacement. (45 hp)
458. Zaman, Patrik, 2015: LiDAR mapping of presumed rock-cored drumlins in the Lake Åsnen area, Småland, South Sweden. (15 hp)
459. Aguilera Pradenas, Ariam, 2015: The formation mechanisms of Polycrystalline diamonds: diamondites and carbonados. (15 hp)
460. Viehweger, Bernhard, 2015: Sources and

effects of short-term environmental changes in Gullmar Fjord, Sweden, inferred from the composition of sedimentary organic matter. (45 hp)

461. Bokhari Friberg, Yasmin, 2015: The paleoceanography of Kattegat during the last deglaciation from benthic foraminiferal stable isotopes. (45 hp)
462. Lundberg, Frans, 2016: Cambrian stratigraphy and depositional dynamics based on the Tomten-1 drill core, Falbygden, Västergötland, Sweden. (45 hp)
463. Flindt, Anne-Cécile, 2016: A pre-LGM sandur deposit at Fiskarheden, NW Dalarna - sedimentology and glaciotectonic deformation. (45 hp)
464. Karlatou-Charalampopoulou, Artemis, 2016: Vegetation responses to Late Glacial climate shifts as reflected in a high resolution pollen record from Blekinge, south-eastern Sweden, compared with responses of other climate proxies. (45 hp)
465. Hajny, Casandra, 2016: Sedimentological study of the Jurassic and Cretaceous sequence in the Revinge-1 core, Scania. (45 hp)
466. Linders, Wictor, 2016: U-Pb geochronology and geochemistry of host rocks to the Bastnäs-type REE mineralization in the Riddarhyttan area, west central Berglsagen, Sweden. (45 hp)
467. Olsson, Andreas, 2016: Metamorphic record of monazite in aluminous migmatitic gneisses at Stensjöstrand, Sveconorwegian orogen. (45 hp)
468. Liesirova, Tina, 2016: Oxygen and its impact on nitrification rates in aquatic sediments. (15 hp)
469. Perneby Molin, Susanna, 2016: Embryologi och tidig ontogeni hos mesozoiska fisködlor (Ichthyopterygia). (15 hp)
470. Benavides Höglund, Nikolas, 2016: Digitization and interpretation of vintage 2D seismic reflection data from Hanö Bay, Sweden. (15 hp)
471. Malmgren, Johan, 2016: De mellankambriska oelandicuslagren på Öland - stratigrafi och faciestyper. (15 hp)
472. Fouskopoulos Larsson, Anna, 2016: XRF -studie av sedimentära borrkärnor - en metodikstudie av programvarorna Q-spec och Tray-sum. (15 hp)
473. Jansson, Robin, 2016: Är ERT och Tidsdomän IP potentiella karteringsverktyg inom miljögeologi? (15 hp)
474. Heger, Katja, 2016: Makrofossilanalys av sediment från det tidig-holocena undervattenslandskapet vid Haväng, östra Skåne. (15 hp)
475. Swierz, Pia, 2016: Utvärdering av vattenkemisk data från Borgholm kommun och dess relation till geologiska förhållanden och markanvändning. (15 hp)
476. Mårdh, Joakim, 2016: WalkTEM-undersökning vid Revingehed provpumpningsanläggning. (15 hp)
477. Rydberg, Elaine, 2016: Gummigranulat - En litteraturstudie över miljö- och hälsopåverkan vid användandet av gummigranulat. (15 hp)
478. Björnfors, Mark, 2016: Kusterosion och äldre kustdyners morfologi i Skälderviken. (15 hp)
479. Ringholm, Martin, 2016: Klimatutlöst matbrist i tidiga medeltida Europa, en jämförande studie mellan historiska dokument och paleoklimatarkiv. (15 hp)
480. Teilmann, Kim, 2016: Paleomagnetic dating of a mysterious lake record from the Kerguelen archipelago by matching to paleomagnetic field models. (15 hp)
481. Schönström, Jonas, 2016: Resistivitets- och markradarmätning i Ängelholmsområdet - undersökning av korrosiva markstrukturer kring vattenledningar. (15 hp)
482. Martell, Josefin, 2016: A study of shock-metamorphic features in zircon from the Siljan impact structure, Sweden. (15 hp)

LUNDS UNIVERSITET

Geologiska institutionen
Lunds universitet
Sölvegatan 12, 223 62 Lund